Lithos 154 (2012) 147–165

Contents lists available at SciVerse ScienceDirect

Lithos

journal homepage: www.elsevier.com/locate/lithos

Geochemistry, geochronology, and Sr–Nd isotopes of the Late Neoproterozoic Wadi Kid volcano-sedimentary rocks, Southern Sinai, Egypt: Implications for tectonic setting and crustal evolution

Abdel-Kader M. Moghazi [a,b], Kamal A. Ali [b,g,*], Simon A. Wilde [c], Qin Zhou [d], Tom Andersen [e], Arild Andresen [e], Mahrous M. Abu El-Enen [f], Robert J. Stern [g]

[a] Department of Geology, Faculty of Science, Alexandria University, Alexandria, Egypt
[b] Department of Mineral Resources and Rocks, Faculty of Earth Sciences, King Abdulaziz University, P.O. Box 80206, Jeddah 21589, Saudi Arabia
[c] Department of Applied Geology, Curtin University, Perth, 6845 WA, Australia
[d] Institute of Geology and Geophysics, Chinese Academy of Sciences, Beijing 10029, China
[e] Department of Geosciences, P.O. Box 1047, University of Oslo, Blindern, 0316 Oslo, Norway
[f] Geology Department, Faculty of Science, Mansoura University, El-Mansoura 35516, Egypt
[g] Geosciences Department, University of Texas at Dallas, 800 W Campbell Rd., Richardson, TX 75080, USA

ARTICLE INFO

Article history:
Received 21 March 2012
Accepted 4 July 2012
Available online 16 July 2012

Keywords:
Arabian–Nubian Shield
Sinai
Neoproterozoic
U–Pb zircon
Sr–Nd isotopes

ABSTRACT

The Kid Group is one of the few exposures of Neoproterozoic metavolcano-sedimentary rocks in the basement of southern Sinai in the northernmost Arabian–Nubian Shield. It is divided into the mostly metamorphosed volcaniclastic Melhaq and siliciclastic Um Zariq formations in the north and the mostly volcanic Heib and Tarr formations in the south. The Heib, Tarr, and Melhaq formations reflect an intense episode of igneous activity and immature clastic deposition associated with core-complex formation during Ediacaran time, but Um Zariq metasediments are relicts of an older (Cryogenian) sedimentary sequence. The latter yielded detrital zircons with concordant ages as young as 647 ± 12 Ma, which may indicate that the protolith of Um Zariq schist was deposited after ~647 Ma but 19 concordant zircons gave a $^{206}Pb/^{238}U$ weighted mean age of 813 ± 6 Ma, which may represent the maximum depositional age of this unit. In contrast, a cluster of 11 concordant detrital zircons from the Melhaq Formation yield a weighted mean $^{206}Pb/^{238}U$ age of 615 ± 6 Ma. Zircons from Heib Formation rhyolite clast define a $^{206}Pb/^{238}U$ weighted mean age of 609 ± 5 Ma, which is taken to approximate the age of Heib and Tarr formation volcanism. Intrusive syenogranite sample from Wadi Kid yields a $^{206}Pb/^{238}U$ weighted mean age of 604 ± 5 Ma. These constraints indicate that shallow-dipping mylonites formed between 615 ± 6 Ma and 604 ± 5 Ma. Geochemical data for volcanic samples from the Melhaq and Heib formations and the granites show continuous major and trace element variations corresponding to those expected from fractional crystallization. The rocks are enriched in large ion lithophile and light rare earth elements, with negative Nb anomalies. These reflect magmas generated by melting of subduction-modified lithospheric mantle, an inference that is further supported by εNd(t) = +2.1 to +5.5. This mantle source obtained its trace element characteristics by interaction with fluids and melts from subducting oceanic crust during the Late Cryogenian time, prior to terminal collision between fragments of East and West Gondwana at ~630 Ma. Positive εNd(t) values and the absence of pre-Ediacaran zircons in all but Um Zariq metasediments indicate minor interaction with Cryogenian and older crust. A model of extensional collapse following continental collision, controlled mainly by lithospheric delamination and slab break-off is suggested for the origin of the post-collision volcanics and granites at Wadi Kid. No evidence of pre-Neoproterozoic sources was found. Kid Group Ediacaran volcanic rocks are compositionally and chronologically similar to the Dokhan Volcanics of NE Egypt, which may be stratigraphic equivalents.

1. Introduction

The Arabian–Nubian Shield (ANS) is a large tract of Neoproterozoic crust exposed in NE Africa and western Arabia (Fig. 1a). It extends south from Egypt to Sudan, Eritrea and Ethiopia on the western flank of the Red Sea and on the eastern flank from Jordan and Israel south through Saudi Arabia and Yemen; Sinai sits near its northern limit. The ANS evolved during most of Neoproterozoic time (870–540 Ma;

* Corresponding author at: Department of Mineral Resources and Rocks, Faculty of Earth Sciences, King Abdulaziz University, P.O. Box 80206, Jeddah 21589, Saudi Arabia. Tel.: +966 2 640 0579; fax: +966 2 695 2095.
E-mail address: alik6588@yahoo.com (K.A. Ali).

0024-4937/$ – see front matter © 2012 Elsevier B.V. All rights reserved.
doi:10.1016/j.lithos.2012.07.003

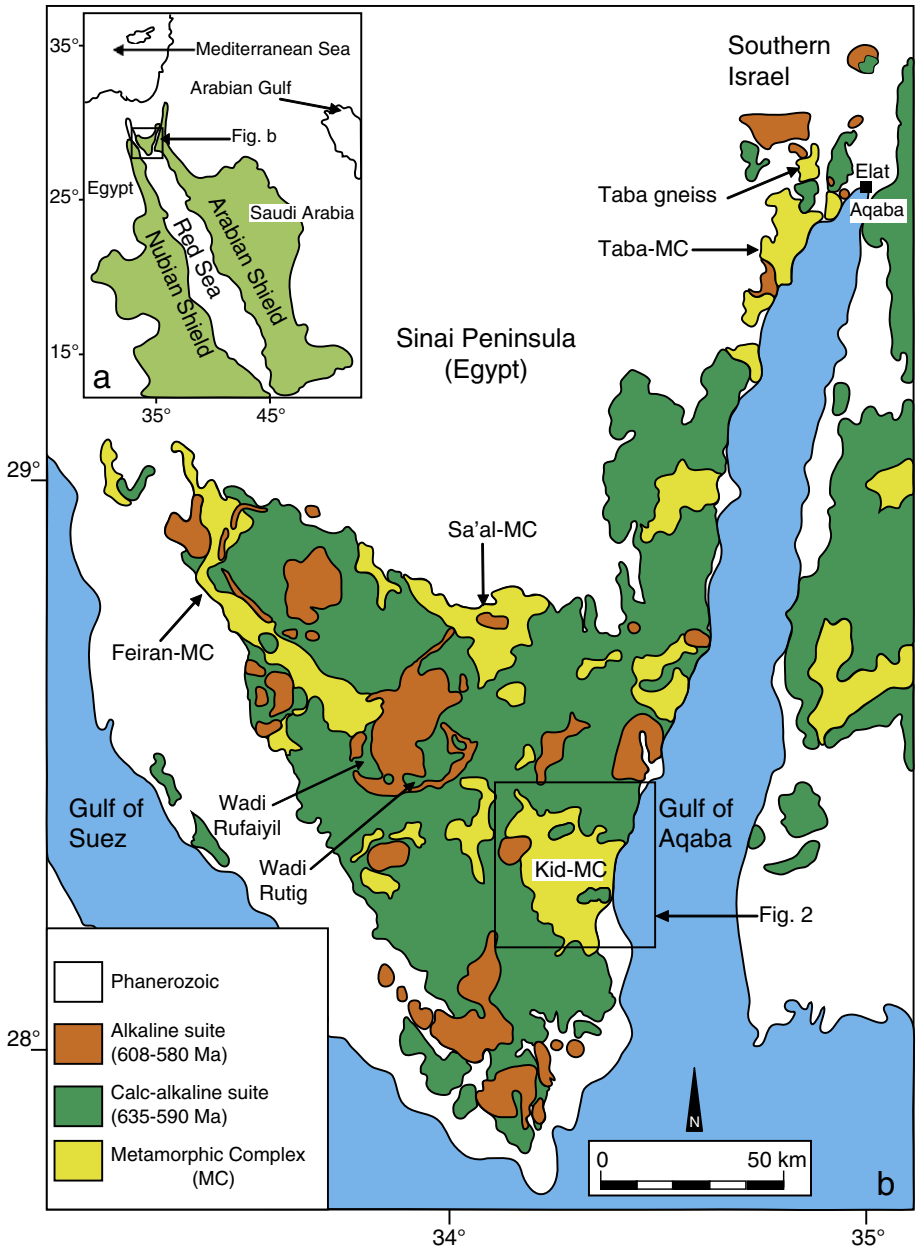

Fig. 1. (a) Simplified map outlining the location of the Arabian–Nubian Shield (ANS). (b) Geological map of Sinai, showing the distribution of the main rock units, the main metamorphic complexes (MC) and the location of the study area.
After Be'eri-Shlevin et al. (2009b) and Eyal et al. (1980).

Stern, 1994), and is generally viewed as a collage of juvenile volcanic arc terranes and ophiolite remnants that were amalgamated during the assembly of Gondwana (Ali K.A. et al., 2009; Genna et al., 2002; Jarrar et al., 2003; Johnson and Woldehaimanot, 2003; Meert, 2003; Stein and Goldstein, 1996; Stern, 2002; Stoeser and Frost, 2006). The ANS is bounded to the east and west by pre-Neoproterozoic crust (Abdelsalam et al., 2002; Johnson and Woldehaimanot, 2003; Sultan et al., 1990; Whitehouse et al., 1998, 2001a, 2001b). The ANS is thus the result of diverse and polyphase geodynamic events and its tectonic evolution can be divided into three major stages, namely: 1) subduction stage (~870–635 Ma) during which island arc volcano-sedimentary sequences and plutonic rocks formed; 2) continental collision (~630–580 Ma, Avigad and Gvirtzman, 2009; Be'eri-Shlevin et al., 2009b) resulting from continuing convergence between East and West Gondwana to form the East African orogen (Stern, 1994), and 3) post-collision stage (580–540 Ma), characterized by stabilization of ANS crust accompanied by the cutting of a vast peneplain (Avigad et al., 2005). The last two stages were accompanied by the development of sedimentary basins (Bentor, 1985; Jarrar et al., 2003; Johnson, 2003; Moghazi, 2003; Stoeser and Camp, 1985) and intrusion of calc-alkaline and alkaline igneous rocks (Beyth et al., 1994; Eyal et al., 2010). The ANS was essentially stable continental crust by early Cambrian time at 530 Ma.

The Neoproterozoic crustal evolution of Sinai (870–550 Ma; Be'eri-Shlevin et al., 2009a, 2009b; Eyal et al., 2010; Kröner et al., 1990, 1994; Moghazi et al., 1998, Stern and Manton, 1987) involved the formation of basins filled with volcano-sedimentary successions engulfed by granitic intrusions (Be'eri-Shlevin, et al. 2011; Brooijmans et al., 2003; Eliwa et al., 2008). The metamorphic complexes (e.g. Taba, Feiran, Sa'al and Kid; Fig. 1b) include infracrustal orthogneiss and supracrustal meta-sedimentary and volcanic sequences, metamorphosed, respectively, at amphibolite and greenschist facies (Abu El-Enen, 2011; Abu

El-Enen et al., 1999, 2004; Abu-Alam and Stuwe, 2009; Eliwa et al., 2008; El-Shafei and Kusky, 2003; Eyal et al., 1980; Katz et al., 1998; Matthews et al., 1989; Shimron, 1984). U–Pb zircon ages for the gneisses are mainly 850–740 Ma, but older metasediments of ~1 Ga and younger gneisses of 660–630 Ma have also been found (Be'eri-Shlevin et al., 2009c; El-Shafei and Kusky, 2003; Eyal et al., 1991; Jarrar et al., 2003; Kolodner et al., 2006; Kröner et al., 1990, 1994; Stern and Manton, 1987). Similar Neoproterozoic volcano-sedimentary successions in the Eastern Desert of Egypt can be classified into a Cryogenian island arc association and an Ediacaran post-collision Dokhan volcanic–Hammamat clastic sediment association (Akaad and Noweir, 1969; El-Gaby et al., 1990). Many authors (e.g. Bentor, 1985; Eyal et al., 1991; Garfunkel, 1999; Shimron, 1980) have inferred Cryogenian island arc (850–760 Ma) volcano-sedimentary and plutonic rocks in the Sinai Peninsula, and several Ediacaran volcano-sedimentary successions (e.g., Kid, Ferani, Rutig, Sa'al-Zaghra, Iqna Shar'a; and Khashabi) are equated with the Dokhan–Hammamat successions of the northern Eastern Desert of Egypt (Azer, 2007; Bentor, 1985; El-Bialy 2010; El-Gaby et al., 1991; Moussa, 2003; Samuel et al., 2001, 2011; Schürmann, 1966; Shimron, 1980).

In this work we focus on possibly correlative volcano-sedimentary successions and post-collision granites exposed in the Wadi Kid area of Sinai (Fig. 1b), which has been the focus of geoscientific studies for the past four decades. We present major and trace element whole-rock geochemistry, coupled with Sr and Nd isotope measurements and zircon U–Pb ages, for felsic volcanic flows (rhyolites), granites and metasedimentary rocks. We use these data to construct a temporal framework for the petrogenesis of magmas in the Kid area and their tectonic setting. This integrated approach advances our understanding of volcano-sedimentary rocks at Wadi Kid and helps to elucidate the tectono-magmatic evolution of the northern ANS.

2. Geologic setting and previous work

Gneisses, metagabbros, metavolcano-sedimentary sequences (Kid Group, Furnes et al., 1985; Shimron, 1984, 1987), albitite (Azer et al., 2010) and granites are exposed in the Wadi Kid area (Fig. 2). The Kid area is dominated by an extension-related igneous and metamorphic core complex (KMC; Blasband et al., 1997, 2000; Brooijmans et al., 2003), although Fowler et al. (2010a, b) argue that KMC evolution was dominated by compressional deformation. Neoproterozoic supracrustal sequences overlie shallow-dipping mylonites developed in the middle crust (Blasband et al., 1997). Post-collisional granites such as the Kid granite (dated here) intrude the mylonite. Gneisses crop out as narrow, elongate NE- to NW-trending masses at the western and eastern margins of the Kid area (Fig. 2). They consist of foliated and lineated quartz diorite and granodiorite. Quartz diorite gneisses are metaplutonic rocks (Be'eri-Shlevin et al., 2009a; Brooijmans et al., 2003), referred to as Quneia Formation by Bentor and Eyal (1987). They have been dated using Rb–Sr techniques at 560–590 Ma (Bielski et al., 1979; Halpern and Tristan, 1981; Moghazi et al., 1998) and with U–Pb zircon at 580–595 Ma (Ali B.H. et al., 2009). Isolated areas of gneissic diorites occur along Wadi Melhaq in the extreme northern part of the area. The Sharira gabbro–diorite complex (Beyth et al., 1978; Mittlefehldt and Ravina, 1983; Moghazi et al., 1998; Shimron,

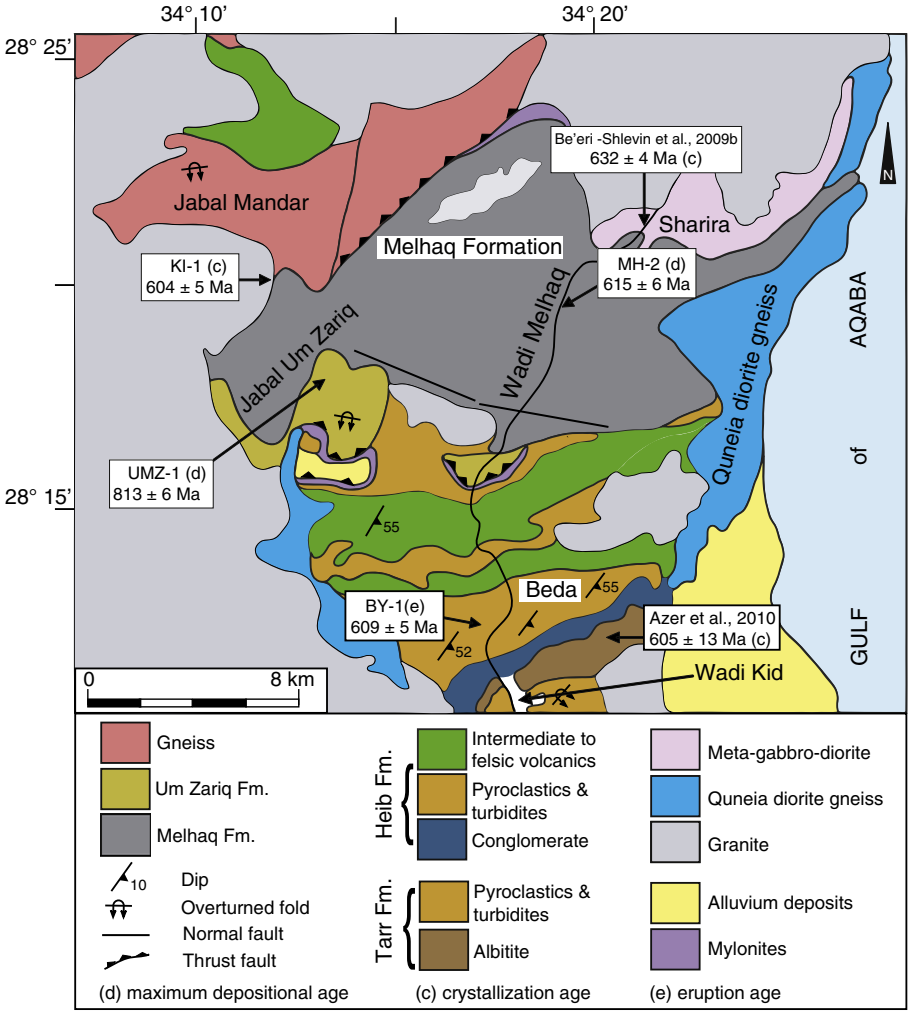

Fig. 2. Geological map of the Wadi Kid area in southeast Sinai, Egypt (after Shimron, 1984), showing the location of samples collected for geochronology studies.

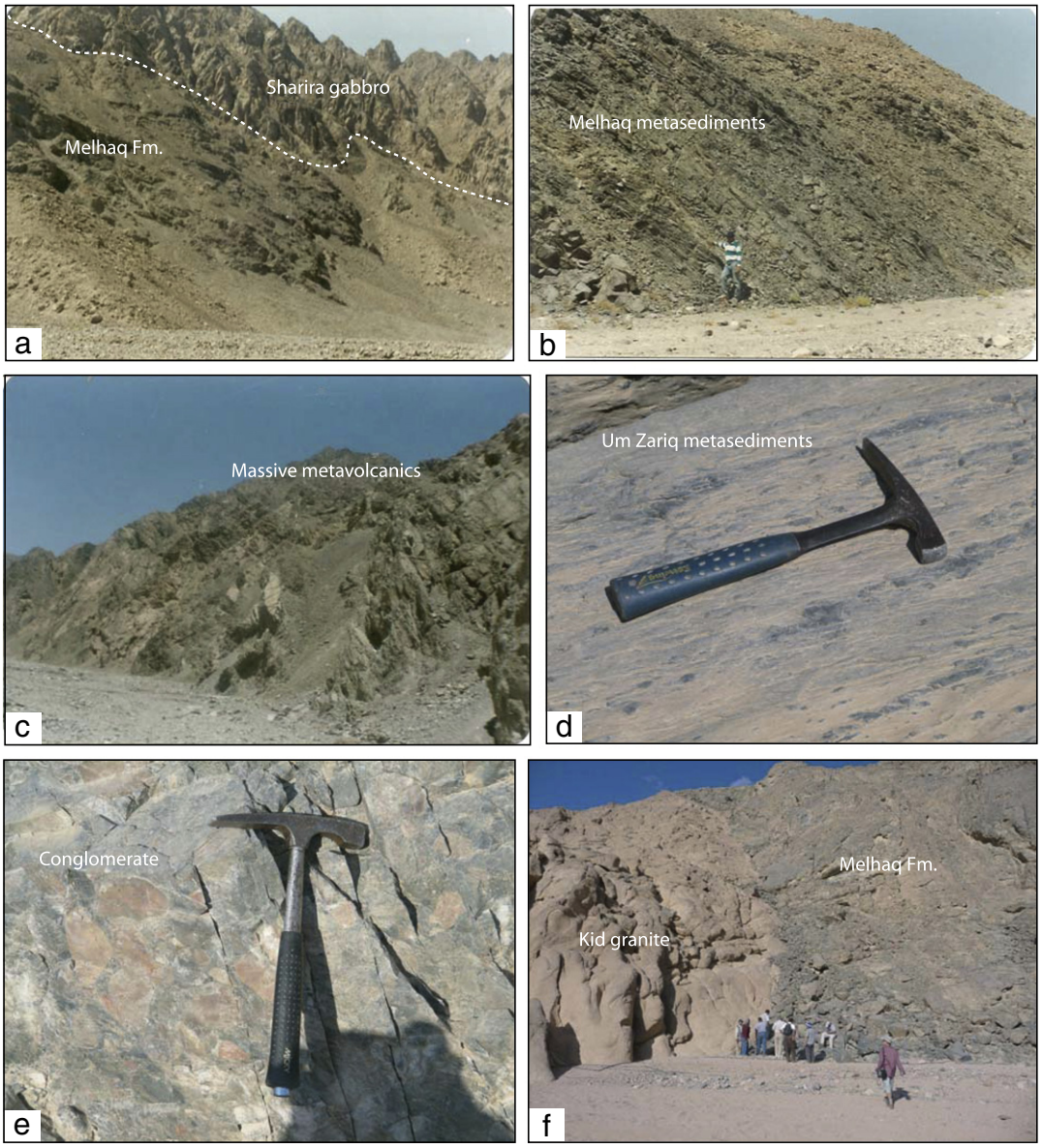

Fig. 3. Field photographs showing field relations and macrostructures of the Kid Group. (a) Irregular intrusive contact between Sharira gabbro–diorite and the Melhaq Formation, (b) metapelitic schist of the Melhaq Formation with strongly foliated and tilted beds defined by compositional layers, (c) massive to weakly foliated Melhaq metavolcanic rocks, (d) metapelitic schist of Um Zariq Formation showing foliation defined by concentration of porphyroblasts, (e) Heib Formation cobble conglomerate, and (f) sharp intrusive contact between Melhaq Formation and Kid granite.

1981, 1984) crops out as a 5 × 15 km NE-trending body along the northern extremity of the Kid area (Fig. 2). The Sharira gabbro–diorite intrudes the Melhaq Formation volcano-sedimentary succession (Fig. 3a) and is intruded by post-collision pink granites along its northern contact (El-Gaby et al., 1991; Hassanen, 1992; Moghazi et al., 1998). The Sharira complex was described by Furnes et al. (1985) as a layered gabbroic and dioritic intrusion and has yielded a U–Pb zircon age of 632 ± 4 Ma (Be'eri-Shlevin et al., 2009a).

Kid Group metasedimentary rocks cover about half of the basement in the Kid area (Fig. 2). Because of deformation, the total thickness of the Kid Group is difficult to determine. Estimates range between >1500 m (Blasband et al., 1997) and 12,000 m (Shimron, 1975, 1987); an intermediate value of 3500 m was proposed by Reymer (1983). Rocks of the Kid Group are folded into a series of ENE–WSW-trending folds affected by greenschist- to amphibolite-facies metamorphism (Abu El-Enen, 2008; Abu El-Enen et al., 2003b; Brooijmans et al., 2003; Eliwa et al., 2004, 2008; Matthews et al., 1989). The grade of metamorphism increases from south to north, where the Kid Group is intruded by the Sharira gabbro–diorite (Atalla, 1989; Blasband et al., 1997). Kid Group metasedimentary and metavolcanic rocks have been dated by Rb–Sr whole-rock techniques at 615 ± 15 Ma by Bielski (1982), though later work suggested a range from 770 to 650 Ma (Blasband et al., 1997; Navon and Reymer, 1984; Reymer et al., 1984). Others workers have correlated the Kid Group with the ~600 Ma Dokhan Volcanics and Hammamat clastic sediments of the Eastern Desert (El-Bialy, 2010; El-Gaby et al., 1991; El-Metwally et al., 1999; Hassanen, 1992).

Shimron (1984, 1987) and Furnes et al. (1985) divided the Kid Group into four formations, namely: the Malhaq and Um Zariq formations in the north and the Heib and Tarr formations in the south. The Malhaq Formation consists of metamorphosed intermediate lavas (andesite and dacite), coarse pyroclastics and finely-bedded tuffs, with conglomerates, pebbly greywackes and pelites. Foliation in the Melhaq Formation varies across the area. Metasedimentary rocks show a well-developed slaty cleavage to schistosity (Fig. 3b), whereas metavolcanics and meta-tuffs are massive and are less foliated (Fig. 3c). The Um Zariq Formation is dominated by quartz-rich metapelites and

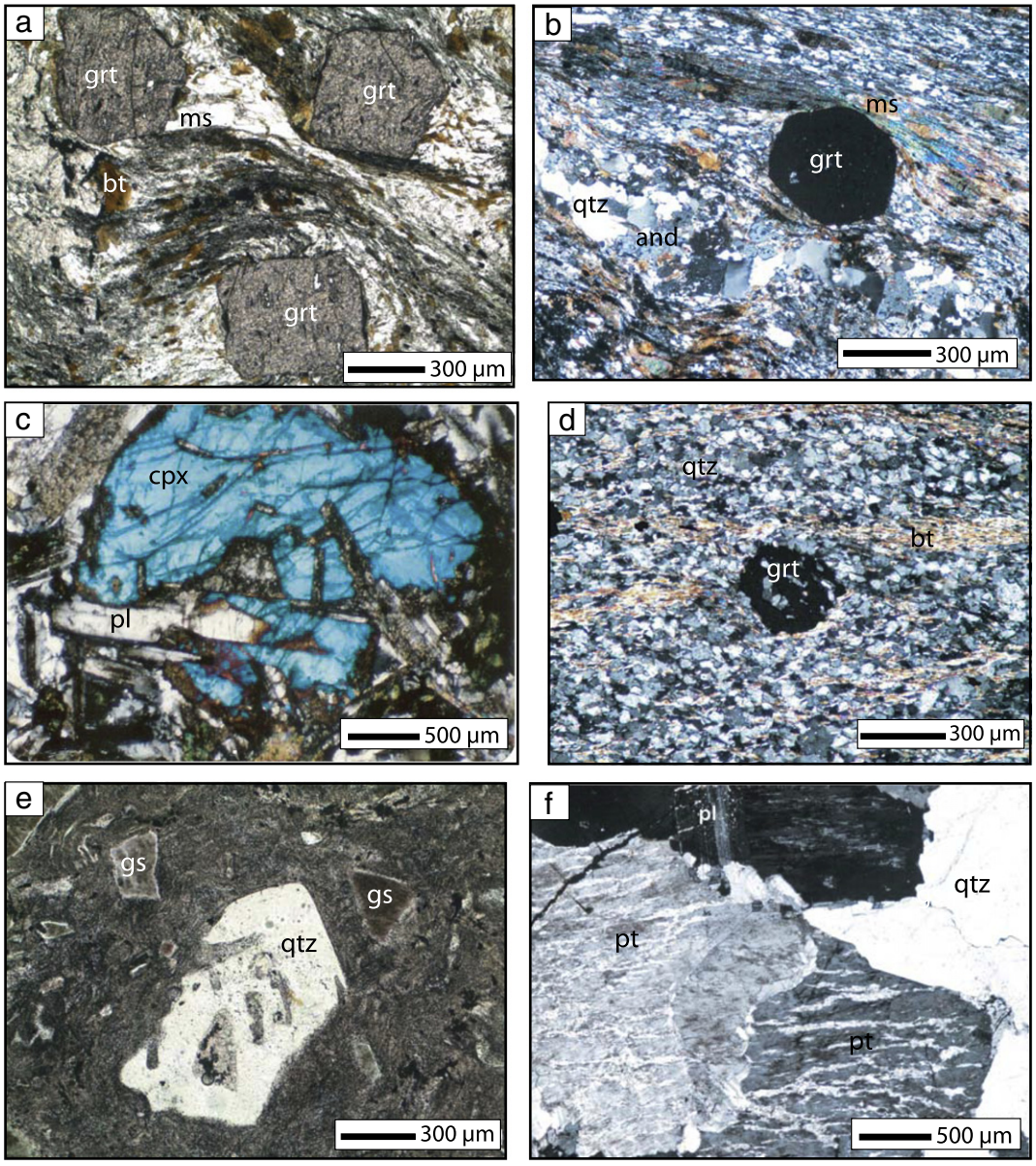

Fig. 4. Photomicrographs of samples studied showing textures and microstructures of the Kid Group and granite. (a) Foliated matrix of quartz, biotite and muscovite wraps around sub-idioblastic garnet porphyroblasts in Um Zariq metasediments, (plane polarized light, PPL), (b) sub-idioblastic andalusite porphyroblasts replaced by muscovite along crystal margins in the Um Zariq metasediments, (crossed polars, XPL), (c) clinopyroxene (augite) phenocryst with ophitic and sub-ophitic texture in a Melhaq Formation andesite (XPL), (d) parallelism of biotite in the Melhaq metasediments (XPL), (e) embayed quartz crystal and glass shards in a welded glassy matrix in an ignimbrite from the Heib Formation (PPL), and (f) perthite, quartz and biotite crystals in a Kid granite (XPL). qtz = quartz, grt = garnet, ms = muscovite, bt = biotite, pl = plagioclase, cpx = clinopyroxene, and = andalusite, gs = glass shard and pt = perthite.

metapsammites interbedded with lithic metagreywackes, meta-tuffs and minor silicic and intermediate lavas. These strongly foliated metasediments (Fig. 3d) have been interpreted as a deep-water flysch sequence that accumulated in an oceanic trench (Shimron, 1980) or as active continental margin shales (Abu El-Enen et al., 2003a, 2003b). The Heib Formation consists of abundant rhyolite and andesite lavas and pyroclastics. In addition, two major NE–SW trending belts of slate and greywacke (Beda Turbidites, Fowler et al. 2010a, b) and cobble and boulder conglomerates with volcanic clasts (Kid Conglomerate, Fig. 3e) are present within the Heib Formation. Some consider these volcanics to have erupted at an active continental margin (El-Gaby et al., 1991; Furnes et al., 1985; Shimron, 1984). Rocks of the Heib Formation are less metamorphosed and deformed than these of the Um Zariq and Malhaq formations. The Tarr Formation in the southern Wadi Kid area is dominantly composed of metaconglomerates, metapelites and metapsammites, along with felsic tuffs and flows. The Tarr Formation is intruded by albitite and carbonatite (Blasy et al., 2001; Shimron, 1975; Soliman et al., 1992) with a U–Pb zircon age of 605 ± 13 Ma (albitite; Azer et al., 2010). Shimron (1983, 1984) inferred that the Tarr Formation formed in a fore-arc, but it may have formed in a rift basin of the sort envisioned in the NE Desert of Egypt by Stern et al. (1984).

Post-collisional granites, mainly monzogranite and syenogranite, represent the last magmatic activity in the areas bordering Wadi Kid (Fig. 2). These are termed Iqna granite by Bielski et al. (1979) and have been dated by Rb–Sr techniques at 570–580 Ma (Bielski et al., 1979; Moghazi et al., 1998). Ion-probe U–Pb zircon dating (Be'eri-Shlevin et al. 2009a) indicates that similar granites from Sinai and southern Israel were emplaced at 580–608 Ma. The granites intrude the Um Zariq,

Melhaq, Heib and Tarr formations with sharp contacts (Fig. 3f) and are themselves intruded by numerous mafic and felsic dykes.

3. Petrography

The petrography of the Kid Group is described below.

The Um Zariq Formation consists of phyllite and mica schist with porphyroblasts of biotite, garnet, cordierite, staurolite and andalusite (Fig. 4a, b). The protoliths of these sediments were quartz-rich aluminous pelites and psammites interbedded with plagioclase-rich lithic greywackes, tuffs and minor lavas of silicic and intermediate composition. Calculated P–T metamorphic conditions (Brooijmans et al., 2003) indicate that Um Zariq metasediments underwent lower amphibolite facies metamorphism (540–558 °C/3–4 kbar).

The Melhaq Formation is composed of metavolcanics (mainly andesite and dacite) and metasediments (including minor conglomerate, pebbly greywacke and pelite). The andesites are porphyritic, with plagioclase (An_{25-30}), augite and hornblende phenocrysts. The groundmass is mostly composed of plagioclase laths and hornblende microlites with subordinate biotite and quartz. Augite phenocrysts, in the form of equant crystals, are characterized by ophitic and sub-ophitic textures (Fig. 4c) and are sometimes pseudomorphed by amphibole. Hornblende phenocrysts are brownish green, anhedral to subhedral and occasionally contain augite relicts. Iron oxides and apatite are the main accessory minerals. Secondary minerals include chlorite, sericite, epidote, and calcite, in order of decreasing abundance. Dacites are mainly made up of plagioclase (An_{12-18}), quartz, minor alkali feldspar, biotite and hornblende together with accessory apatite, titanite, and Fe-oxides. Pyroclastic rocks are mainly andesitic and dacitic crystal tuffs, composed of crystals (up to 0.5 mm long) of plagioclase and hornblende, together with a few volcanic rock fragments (up to 0.2 mm). Crystal and rock fragments are set in a tuffaceous cryptofelsitic matrix primarily composed of quartz and feldspar, with streaks of chlorite, biotite and calcite together with minor epidote, Fe-oxides, apatite and titanite. The metasediments are typically foliated, mica-rich phyllites and schists (Fig. 4d). They contain sporadic porphyroblasts of garnet, cordierite and magnetite in a matrix of biotite, muscovite, quartz, plagioclase, with magnetite and occasionally tourmaline. Calculated P–T metamorphic conditions (Abu El-Enen, 2008; Brooijmans et al., 2003; Eliwa et al., 2004, 2008) indicate greenschist to lower amphibolite facies (480–570 °C/

Table 1
Major and trace element data for representative samples from Wadi Kid, Sinai, Egypt.

Sample	Melhaq volcanics		Heib Volcanics		Kid granite		Metapelitic schist	
	MV42-2*	MV25-2*	HV522*	BY-1**	K11-1**	KI-1**	UMZ-1**	MH-2**
SiO_2	55.12	58.11	70.55	77.48	73.89	73.88	60.66	74.65
TiO_2	1.09	1.08	0.41	0.19	0.18	0.18	1.00	0.34
Al_2O_3	16.57	16.14	15.25	12.07	13.66	13.62	21.70	12.46
Fe_2O_3	7.58	7.62	2.20	1.84	1.62	1.56	6.44	3.41
MnO	0.12	0.11	0.12	0.04	0.05	0.04	0.30	0.07
MgO	5.56	3.64	0.50	0.14	0.15	0.13	0.94	1.01
CaO	6.89	5.48	1.39	1.44	0.79	0.77	1.12	1.61
Na_2O	3.43	3.91	4.79	4.89	3.86	3.85	1.41	1.69
K_2O	1.80	1.90	3.71	0.94	5.34	5.40	3.29	2.60
P_2O_5	0.29	0.28	0.11	<0.01	0.02	0.03	0.04	0.05
LOI	1.27	1.68	0.44	0.80	0.30	0.40	2.80	1.80
AI	Nc	Nc	Nc	Nc	1.00	1.01	Nc	Nc
Mg#	68	58	39	18	Nc	Nc	Nc	Nc
Cr	122	119	103	<14	<14	<14	89	21
Ni	87	41	5	20	20	20	20	20
Sc	19	15	4	3	2	2	22	8
Co	32	31	2	1.5	43	46	11	7
V	193	166	23	9	10	8	127	47
Cs	2.1	3.5	4.4	2.5	1.9	1.9	6.4	1.6
Ba	515	668	787	438	396	387	1115	1367
Rb	43	45	114	21	176	181	72	52
Sr	769	701	309	390	84	84	137	95
Ga	22	14	27	16	21	21	26	18
Hf	4.9	4.3	5.2	9.0	7.7	7.3	7.1	7.3
Nb	6.0	5.0	12.0	14.0	25.7	27.4	10.8	11.7
Zr	199	179	181	288	240	207	228	255
Y	21	21	26	29	36	40	41	45
Ta	0.72	0.65	0.85	0.90	2.20	2.10	0.90	0.80
Th	4.80	3.23	11.40	14.70	13.10	14.20	10.40	7.70
U	1.70	1.28	3.23	4.30	2.80	3.10	3.30	1.80
La	27.58	27.52	31.80	30.50	51.70	58.10	54.20	42.30
Ce	63.86	48.07	66.38	68.30	106.90	125.40	112.20	94.70
Pr	NA	NA	NA	8.41	12.83	14.49	13.35	11.89
Nd	29.72	24.60	27.82	32.50	47.30	50.10	50.80	48.20
Sm	5.23	4.21	4.42	6.30	7.85	8.87	9.20	9.95
Eu	1.41	1.35	0.83	0.48	1.04	1.07	1.74	1.54
Gd	4.12	3.75	2.59	5.38	6.07	6.80	7.98	7.91
Tb	0.59	0.54	0.42	0.93	1.06	1.18	1.35	1.31
Dy	NA	NA	NA	5.23	6.09	6.79	7.77	7.64
Ho	0.80	0.75	0.58	1.11	1.26	1.47	1.59	1.59
Er	NA	NA	NA	3.14	3.70	4.13	4.50	4.38
Tm	NA	NA	NA	0.51	0.60	0.66	0.68	0.73
Yb	2.08	1.80	1.82	3.42	4.35	4.75	4.10	4.46
Lu	0.32	0.27	0.30	0.49	0.64	0.69	0.62	0.73

Major (wt.%) and trace (ppm). Fe_2O_3 = total FeO and NA = not analyzed.
[Agpaitic index (AI) = (Na + K)/Al]; Nc = not calculated. Mg# = (100 Mg/(Mg + Fe^{2+})).
* Samples analyzed at the Mineralogical–Geological Museum, University of Oslo, Norway using XRF (major and trace elements) and INNA (REE).
** Samples analyzed at ACME Analyrical Lab., Canada by ICP-AES (major elements) and ICP-MS (trace and REE).

Table 2
Nd and Sr isotopic data for granitic and volcanic rocks from Wadi Kid, Sinai.

Sample	Unit	U–Pb zircon age (Ma)	Rb ppm	Sr ppm	$^{87}Rb/^{86}Sr$	$^{87}Sr/^{86}Sr \pm 2\sigma$	$^{87}Sr/^{86}Sr$ (initial)	Sm ppm	Nd ppm	$^{147}Sm/^{144}Nd$	$^{143}Nd/^{144}Nd \pm 2\sigma$	$^{143}Nd/^{144}Nd$ (initial)	eNd (initial)	Nd model age (Goldstein et al., 1984) (Ga)	Nd model age (DePaolo, 1981) (Ga)
K108	Kid granite	604 ± 5	119	14	24.64	0.903860 ± 34	0.691645	4.5	23.7	0.1140	0.512550 ± 25	0.512099	4.68	0.92	0.76
K124			80	111	2.09	0.720488 ± 29	0.702482	5.3	36.5	0.0881	0.512433 ± 24	0.512084	4.39	0.87	0.75
K130			146	84	5.03	0.744305 ± 22	0.700937	6.2	45.9	0.0821	0.512415 ± 65	0.512090	4.50	0.85	0.74
K153			80	260	0.89	0.710700 ± 11	0.703026	8.1	46.8	0.1053	0.512550 ± 23	0.512133	5.35	0.85	0.71
K161			152	91	4.82	0.742523 ± 13	0.701012	6.9	50.7	0.0830	0.512422 ± 26	0.512093	4.57	0.85	0.73
K202			112	211	1.54	0.715805 ± 21	0.702578	13.5	72.2	0.1137	0.512545 ± 12	0.512095	4.60	0.92	0.77
MV26-2	Melhaq volcanic	632 ± 4[a]	38	722	0.15	0.704001 ± 7	0.702604	5.7	26.0	0.1347	0.512537 ± 5	0.511979	3.04	1.19	0.98
MV361			57	613	0.27	0.705336 ± 8	0.702911	5.7	24.8	0.1393	0.512632 ± 9	0.512055	4.53	1.06	0.85
MV382			45	763	0.17	0.704346 ± 29	0.702819	6.9	28.8	0.1448	0.512649 ± 9	0.512049	4.41	1.11	0.88
MV385			35	803	0.13	0.703783 ± 9	0.702650	5.7	26.5	0.1308	0.512644 ± 9	0.512102	5.45	0.93	0.75
HV12-2	Heib volcanic	609 ± 5	132	63	6.08	0.754529 ± 12	0.701773	6.7	29.1	0.1398	0.512532 ± 6	0.511975	2.36	1.28	1.06
HV46-2			99	146	1.98	0.719764 ± 15	0.702587	3.8	24.2	0.0957	0.512491 ± 21	0.512110	4.99	0.85	0.72
HV82			105	116	2.62	0.724895 ± 9	0.702193	5.3	31.4	0.1029	0.512373 ± 26	0.511963	2.12	1.07	0.93
HV426			93	418	0.64	0.708503 ± 7	0.702965	4.7	24.4	0.1168	0.512546 ± 8	0.512081	4.42	0.95	0.79

Sr and Nd isotopic analyses and element concentrations undertaken at the Mineralogical–Geological Museum, University of Oslo, Norway using a VG354 and a Finningan Mat 262 solid source instrument. Model ages based on DePaolo (1981) and Goldstein et al. (1984). eNd(T) and initial $^{87}Sr/^{86}Sr$ were calculated using U–Pb zircon ages obtained during this study except for [a]age from Be'eri-Shlevin et al. (2009b). Mean values JM standards is $^{143}Nd/^{144}Nd = 0.511101 \pm 0.000015$ and NBS 987 standards is $^{87}Sr/^{86}Sr = 0.710228 \pm 0.000040$. Sr and Nd of Kid granite data from Moghazi et al. (1998), are re-calculated using the U–Pb zircon age obtained during this study. Analytical uncertainties in $^{87}Rb/^{86}Sr$ and $^{87}Sr/^{86}Sr$ used to weight the regression and to calculate the MSWD are 1 and 0.02%, respectively.

3–4 kbar), except in the extreme northeastern part, which reached upper amphibolite facies (645 °C/4.5–5.5 kbar).

The Heib and Tarr Formations are mixed sequences of metasediments and metavolcanics. The metasediments contain a thick sequence of turbiditic slate and greywacke (Beda Turbidites), with cobble and boulder conglomerate beds and lenses with rhyolite clasts. The volcanic rocks include dacite, rhyodacite and rhyolite. Dacites and rhyodacites contain phenocrysts of plagioclase, quartz, K-feldspar, and occasional hornblende and biotite, embedded in a microcrystalline matrix of dense aggregates and granules of the same minerals. Rhyodacite and dacite can be distinguished on the basis of modal quartz and ferromagnesian minerals. There are three types of rhyolite: rhyolite porphyry (dominant), aphyric rhyolite, and ignimbrite. The porphyritic rhyolite is characterized by phenocrysts of subhedral K-feldspar, quartz, and plagioclase (up to 8 × 3 mm) in an aphanitic groundmass. The groundmass consists of quartz, K-feldspar, biotite, titanite, zircon and Fe-oxides. The less common aphyric rhyolite is akin to the porphyritic variety, but with a granular texture. The ignimbrite is mineralogically similar to the other rhyolitic varieties but differs in having altered glass shards and pumaceous fragments (Fig. 4e) displaying flow texture, thus indicating that it was an ignimbrite. Blasband (1995) estimated metamorphic conditions of 350–400 °C and 2–3 kbar for the Beda Turbidites and noted that cordierite appears in the more westerly exposures. Brooijmans (1996) and Brooijmans et al. (2003) described local upper greenschist to lower amphibolite facies assemblages in the Heib Formation, including cordierite.

Post-collisional granites are predominantly pale pink to red syenogranites. They are massive and equigranular, but porphyritic outcrops with large (up to 1.5 cm) K-feldspar crystals are also present. They are subsolvus granitic rocks (Fig. 4f) consisting of quartz (35%), perthitic orthoclase (35%), and plagioclase (An_{10-15}, 28%), together with biotite and hornblende (2%) and accessory magnetite, ilmenite, titanite, apatite and zircon. Plagioclase inclusions in large quartz crystals are common. Late-stage muscovite and chlorite locally replace biotite.

4. Analytical techniques

Major and trace element analyses of 34 samples from the Melhaq and Heib volcanic rocks were performed at the Mineralogical–Geological Museum, University of Oslo, Norway, on fused and powder pellets, using a Philips PW 2400 X-Ray Fluorescence instrument with an end-window Rh tube. The rare earth elements (REE), Cs, Hf, Ta, Th and U were determined by Instrumental Neutron Activation (INNA) using coaxial HP Ge detector at the Mineralogical–Geological Museum, University of Oslo, Norway. Another two metasediment and six granite samples were analyzed at the ACME Analytical Laboratories Ltd., Canada. Major elements and Sc, Ba, and Ni abundances were determined by inductively-coupled plasma-atomic emission spectrometry (ICP-AES) after fusing 0.2 g of sample powder using $LiBO_2$. Other trace elements including REE were determined by inductively-coupled plasma-mass spectrometry (ICP-MS). Chemical data are listed in Table A1 (Supplementary materials) and representative analyses are given in Table 1.

Isotopic compositions of Sr and Nd and the concentrations of Rb, Sr, Sm and Nd in 8 volcanic samples were determined by mass spectrometry at the Mineralogical–Geological Museum, University of Oslo, Norway (Table 2). Concentrations of these elements and $^{87}Sr/^{86}Sr$ were determined using a VG 354 5 collector TIMS instrument, while isotopic compositions of Nd were determined using a Finnigan MAT 262, 9 collector TIMS. Replicate analyses of NBS 987 standard (n = 19) yielded a mean $^{87}Sr/^{86}Sr$ of 0.710228 ± 50 (2σ) while the JM Nd standard (n = 45) yielded $^{143}Nd/^{144}Nd$ of 0.511101 ± 15 (2σ). Initial $^{143}Nd/^{144}Nd$ was calculated for individual samples expressed as εNd(t) using $^{147}Sm/^{144}Nd = 0.1967$ and $^{143}Nd/^{144}Nd = 0.512638$ for the present bulk Earth (Allégre et al., 1983). The decay constant used for ^{147}Sm was 6.54×10^{-12} y^{-1} and for ^{87}Rb is 1.42×10^{-11} y^{-1}. Model Nd ages (T_{DM}) were calculated according to the depleted mantle models of DePaolo (1981) and Goldstein et al. (1984). The Melhaq and Heib volcanics were dated using Rb–Sr whole-rock techniques. Rb/Sr isochron age was calculated using the Isoplot software package (Ludwig, 2001a). All uncertainties are 2σ, and age errors are given with 95% confidence limits.

Four samples were collected from the Um Zariq and Melhaq metasediments, Heib rhyolite and Kid granite for zircon U–Pb age determinations. Zircons were separated at the University of Texas at Dallas (UTD) using standard crushing, heavy liquid and magnetic separation techniques. Grains from the non-magnetic fractions were hand-picked, mounted on double-sided adhesive tape, and set in Epirez™ resin. Mounted zircons were ground and polished to effectively cut them in half and then were imaged by cathodoluminescence (CL) using a scanning electron microscope prior to gold coating in order to highlight

any internal structures. U–Th–Pb analyses were performed on the four samples using an Agilent 7500a Q-ICPMS connected to a 193 nm Excimer laser ablation system at the Institute of Geology and Geophysics, Chinese Academy of Sciences, Beijing following techniques described by Xie et al. (2008). One spot was measured on each of 99 zircons, along with 43 analyses of the 91,500 standard and 21 analyses of the GJ-1 standard (Table A3 — supplementary data). The relative standard deviations of reference values for the 91,500 standard were set at 2%. Data were processed using the SQUID (Ludwig, 2001b) and Isoplot (Ludwig, 2001a) software. The $^{206}Pb/^{238}U$ ages are most reliable for young zircons and are utilized here. This reflects the fact that low count rates for ^{207}Pb result in large uncertainties and therefore $^{207}Pb/^{206}Pb$ is less sensitive

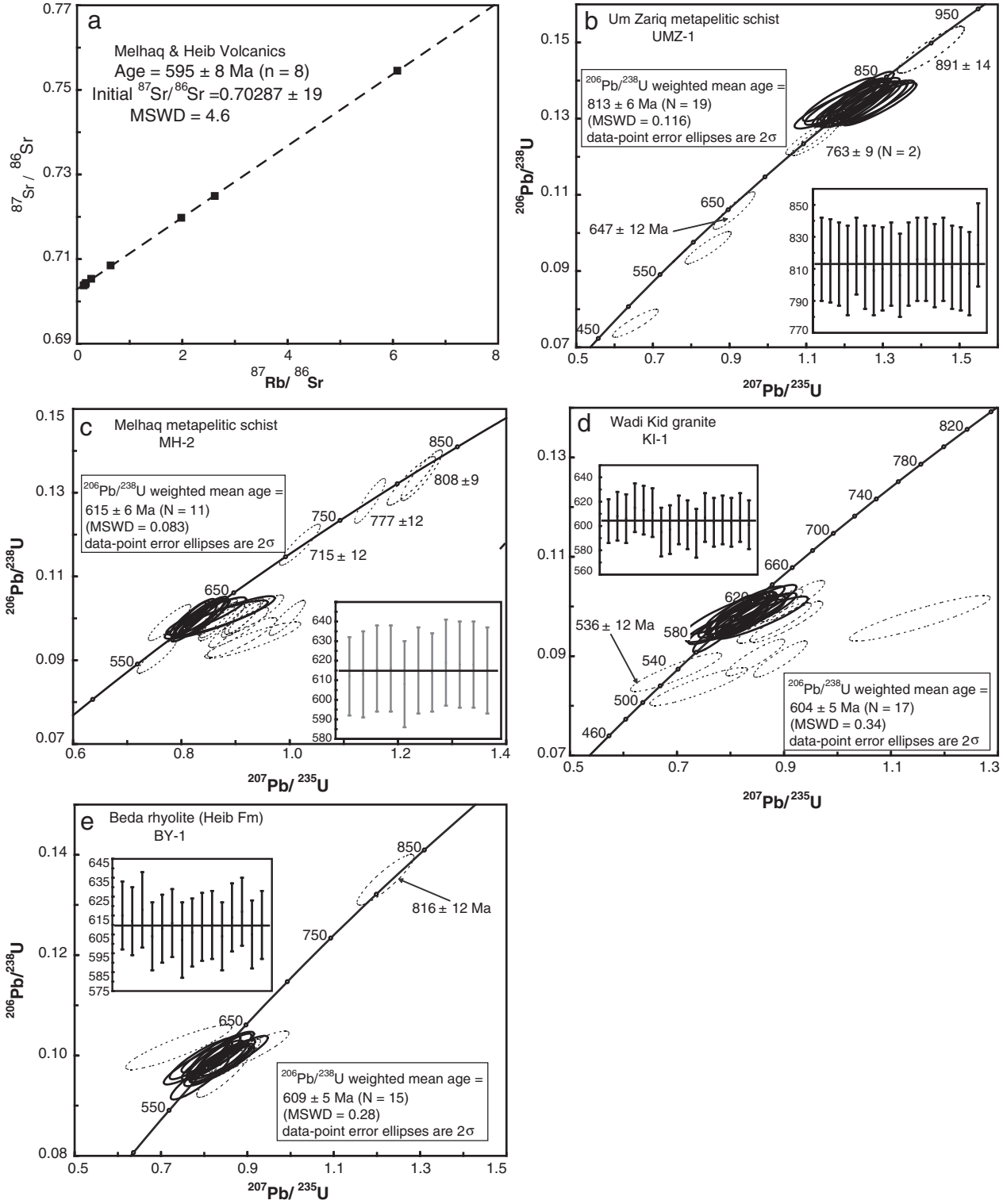

Fig. 5. (a) Rb–Sr whole-rock (WR) errorchron diagram of all Heib and Melhaq volcanic rocks analyzed in this study. (b) U–Pb concordia diagram for LA-ICP-MS data from Um Zariq metapelitic schist UmZ-1. (c) U–Pb concordia diagram for LA-ICP-MS data from Melhaq metapelitic schist sample MH-2. (d) U–Pb concordia diagram for LA-ICP-MS data from Wadi Kid granite sample KI-1. (e) U–Pb concordia diagram for LA-ICP-MS data from Beda rhyolite (Heib Formation) sample BY-1. Dashed ellipses indicate zircon analyses that were excluded from age calculations. Analytical data are given in Table A2 (Supplementary data).

measure of age for young (<1.0 Ga) zircons (Black et al., 2004; Compston et al., 1992).

5. Geochronology

5.1. Rb/Sr geochronology

The $^{87}Rb/^{86}Sr$, $^{87}Sr/^{86}Sr$, $^{147}Sm/^{144}Nd$ and $^{143}Nd/^{144}Nd$ ratios, together with the initial $^{87}Sr/^{86}Sr$, εNd and T_{DM} model ages for 8 samples of the Melhaq and Heib volcanics are given in Table 2. Regression of all eight samples yields an errorchron age of 595 ± 8 Ma (MSWD = 4.6), with initial $^{87}Sr/^{86}Sr = 0.70287 \pm 19$ (Fig. 5a). Accepting Sr_i for 7 samples with $^{87}Rb/^{86}Sr < 3$, Sr_i ranges from 0.70219 to 0.70296 (Table 2) with a mean of 0.70265 ± 0.00026 (one standard deviation), which is similar to that expected for magmas extracted from Neoproterozoic depleted mantle and much lower than what would be expected if there was even minor involvement of pre-Neoproterozoic continental crust (Liégeois and Stern, 2010). The Rb–Sr errorchron age is slightly younger than U/Pb zircon ages (see below) but it is not considered to be a reliable age.

5.2. U–Pb zircon geochronology

5.2.1. Um Zariq metasediments

Zircons extracted from a metapelitic schist sample UMZ-1 (28° 18′ 27.6″ N; 34° 15′ 09.1″ E) are mostly euhedral to subhedral, although some are rounded and pale brown in color. In CL images some grains show oscillatory zoning whereas others have weak to no zoning (Fig. 6a). One measurement was made on each of 25 zircons (Table A2 — supplementary materials) and these are presented on a concordia plot (Fig. 5b). Two spots (9 and 16) are discordant. Spot 18 yields a concordant $^{206}Pb/^{238}U$ age of 647 ± 12 Ma, which is younger than the other analyses. Two spots (2 and 22) yield a $^{206}Pb/^{238}U$ mean age of 763 ± 9 Ma and spot 4 records an older $^{206}Pb/^{238}U$ age (891 ± 41 Ma). The remaining nineteen analyses yield a $^{206}Pb/^{238}U$ weighted mean age of 813 ± 6 Ma (MSWD = 0.116; Fig. 5b). One interpretation is that the protolith of this schist was deposited and lithified sometime after ~647 Ma. Another interpretation is that this age represents lead loss and that the maximum sediment age is better represented by the cluster of 19 zircons at 813 ± 6 Ma. This age cluster broadly fits with the common age range of 740–850 Ma for Sinai metamorphic complexes (Eyal et al., 1991; Kröner et al., 1990) and with the age of major crustal components elsewhere in the ANS (e.g. Stern, 1994).

5.2.2. Melhaq metasediments

Zircons extracted from metapelitic schist sample MH-2 (28° 18′ 59.4″ N; 34° 19′ 23″ E) are mostly euhedral to subhedral and pale brown in color. CL images show faint zoning, but some are unzoned (Fig. 6b). One measurement was made on each of 27 zircons (Table A2 — supplementary materials) and these results are presented on a

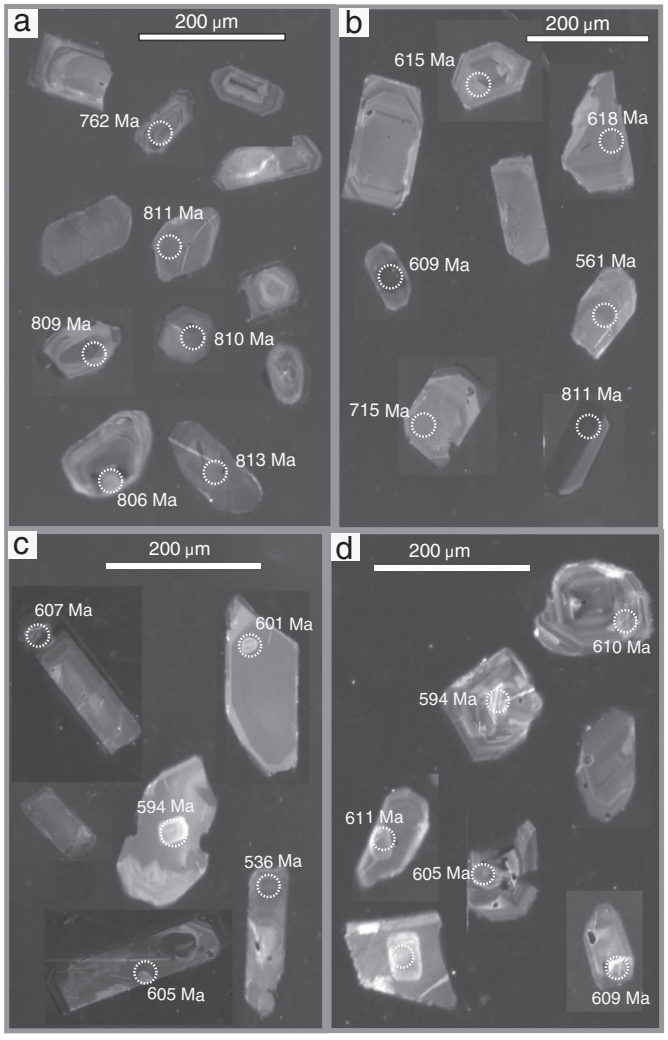

Fig. 6. Cathodoluminescence (CL) images of zircons from samples analyzed in this study. (a) Um Zariq metapelitic schist sample # UMZ-1. (b) Melhaq metapelitic schist sample # MH-2. (c) Wadi Kid granite sample # KI-1. (d) Beda rhyolite sample # BY-1. Location of LA-ICP-MS U–b sites (30 μm) shown by white dotted circles.

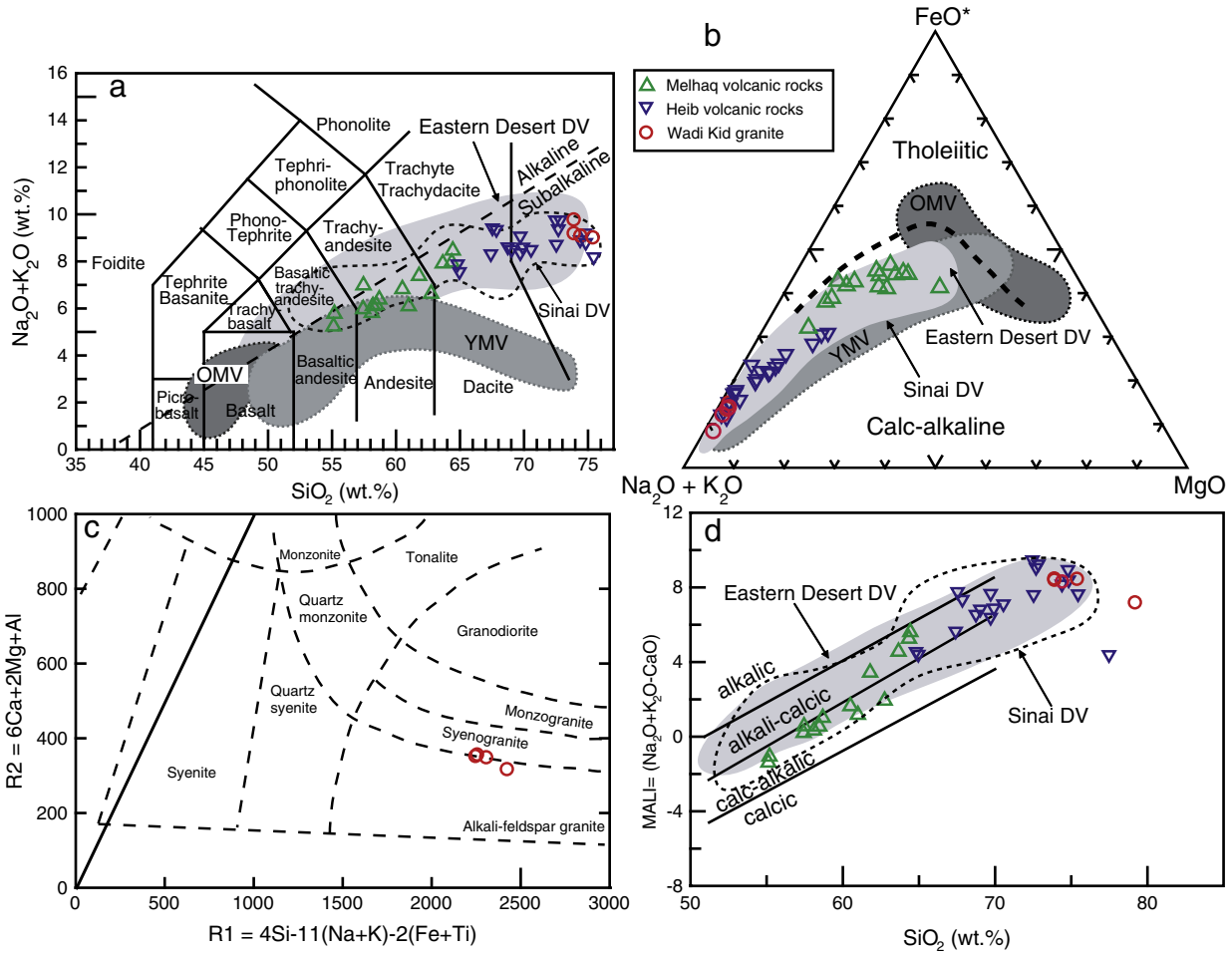

Fig. 7. (a) Total alkalis vs. silica diagram of Le Bas et al. (1986), showing the classification of Kid Group volcanics. (b) A (Na_2O+K_2O wt.%)-F (total Fe as FeO wt.%)-M (MgO wt.%) classification diagram of Irvine and Baragar (1971), showing the Kid Group volcanics, plotting in the calc-alkaline field. (c) R1–R2 diagram (de La Roche et al., 1980), showing the Kid granite samples plot in the alkali-feldspar granite and syenogranite fields. (d) MALI (modified alkali lime index) vs. SiO_2 (after Frost et al., 2001). Sinai DV include data for Ediacaran lavas from Rutig (Be'eri-Shlevin et al., 2011), Kid Volcanics (El-Bialy, 2010), and Wadi Rufaiyil (Azer and Farahat, 2011).
In (a) and (b) the fields of ophiolitic metavolcanics (older metavolcanics, OMV), island arc metavolcanics (younger metavolcanics, YMV) and Dokhan Volcanics (DV) are from Ali K.A. et al. (2009), Abdel Rahman (1996), Basta et al. (1980), Eliwa et al. (2006), Moghazi (2003), Stern (1981), and Stern and Gottfried (1986).

concordia plot (Fig. 5c). Twelve spots are discordant and are excluded from further discussion. Spots 18 and 6 are concordant and yield $^{206}Pb/^{238}U$ ages of 715 ± 12 Ma and 777 ± 12 Ma, respectively. Two spots (19 and 22) yield a $^{206}Pb/^{238}U$ mean age of 808 ± 9 Ma (MSWD = 0.43), similar to the Um Zariq zircon ages. These Cryogenian ages broadly fit with that commonly reported for metamorphic complexes in Sinai (ca. 740–850 Ma). The remaining eleven analyses yield a $^{206}Pb/^{238}U$ weighted mean age of 615 ± 6 Ma (MSWD = 0.083). Accordingly, we infer that the protolith of the Melhaq Formation was deposited some time after ~615 Ma.

5.2.3. Wadi Kid granite

Zircons extracted from granite sample KI-1 (28° 19′ 49.83″ N; 34° 12′ 33.40″ E) are mostly euhedral prismatic and pale brown in color. CL images (Fig. 6c) show faint zoning for some zircons, but others show no zoning at all. One measurement was made on each of 27 zircons (Table A2 – supplementary materials) and these results are presented on a concordia diagram (Fig. 5d). Nine analyses are discordant and are not discussed further. Spot 26 is concordant with a $^{206}Pb/^{238}U$ age of 536 ± 12 Ma, which is younger than other analyses but probably reflects Pb-loss, since the grain appears to have undergone recrystallization (Fig. 6c). The remaining seventeen analyses yield a $^{206}Pb/^{238}U$ weighted mean age of 604 ± 5 Ma (MSWD = 0.34; Fig. 5d), which is taken to be the granite crystallization age.

5.2.4. Heib volcanics

Zircons extracted from a rhyolite clast BY-1 (28° 12′ 28.1″ N; 34° 17′ 53.5″ E), collected from Beda pyroclastic rhyolite flows, are mostly euhedral prismatic and pale brown in color. CL images (Fig. 6d) show well-developed oscillatory zoning, typical of magmatic zircons (Corfu et al., 2003). One measurement was made on each of 20 zircons (Table A2 — supplementary materials) and these are presented on concordia diagram (Fig. 5e). Spot 1 is concordant with a $^{206}Pb/^{238}U$ age of 816 ± 12 Ma and is older than other spots, indicating that it is inherited from Cryogenian rocks in the region, such as the Um Zariq metasediments. Four analyses are discordant and are not discussed further. The remaining 15 analyses yield a $^{206}Pb/^{238}U$ weighted mean age of 609 ± 5 Ma (MSWD = 0.28; Fig. 5e), which is taken to record the time of eruption. This age is identical, within uncertainty, to the ages of the Kid granite, the Tarr albitite (Azer et al., 2010), and the Melhaq Formation.

6. Whole rock geochemistry

6.1. Effects of alteration

Although volcanic rocks of the Kid Group have been affected by low temperature metamorphism, as indicated by the formation of chlorite, calcite, actinolite–hornblende, epidote and sericite at the expense of ferromagnesian minerals and feldspars, original minerals (augite,

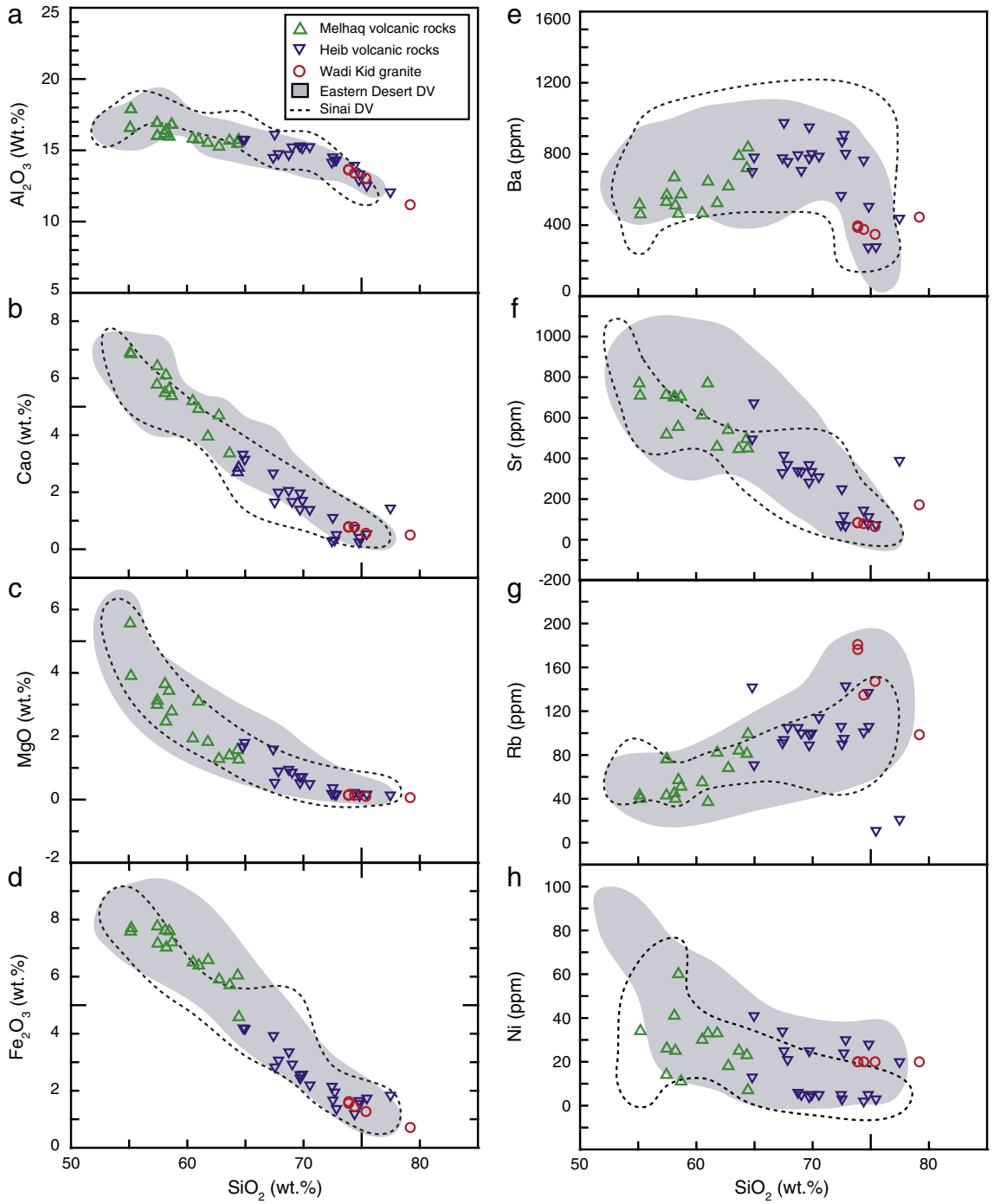

Fig. 8. Harker variation diagrams of some major and trace elements of the Kid Group volcanic rocks. Sinai DV (dashed field) include data for Ediacaran lavas from Rutig (Be'eri-Shlevin et al., 2011), Kid Volcanics (El-Bialy, 2010), and Wadi Rufaiyil (Azer and Farahat, 2011).
Gray field is for Dokhan Volcanics in the Eastern Desert with data from Abdel Rahman (1996), Eliwa et al. (2006), Moghazi (2003), and Stern and Gottfried (1986).

plagioclase, K-feldspar and biotite) and primary volcanic textures are still preserved. However, it cannot be assumed that the chemical composition of the investigated volcanic rocks was not changed as a result of metamorphism. Different elements show different degrees of mobility during metamorphism (Humphris, 1984; Polat and Hofmann, 2003; Polat et al., 2003; Winchester and Floyd, 1976). Alkaline earths such as Ca, Sr and Ba and alkali metals such as Na, Rb and K are commonly mobilized during post-magmatic alteration and metamorphism (e.g. Polat et al., 2007). In contrast, REE, HFSE, some transition metals and Th are relatively immobile during alteration (e.g. Humphris, 1984; Winchester and Floyd, 1976). Thus, to avoid the effects of secondary remobilization, careful selection of samples in the field and by microscopic examination identified the least altered samples for chemical analysis. Chemical variation diagrams of most major and trace elements (see below) show little scatter, suggesting limited element mobility. Another criteria used to assess the effect of alteration on volcanic rocks from the Wadi Kid follow the suggestion of Polat and Hofmann (2003) that samples with Loss On Ignition (LOI) > 6 wt.% and Ce/Ce* ratios greater than 1.1 and less than 0.9 are highly altered and should be avoided. All Wadi Kid volcanics have LOI between 2.01 and 0.21 wt.% and Ce/Ce*

from 1 to 1.1 (Table A1, supplementary materials) further suggesting that they are not severely affected by subsequent metamorphism.

6.2. Major element variations

Volcanic rocks of the Kid Group are a broadly dacitic calcalkaline suite, with 55.1–77.5 wt.% SiO_2 showing a subalkaline trend on the total alkali vs. silica (TAS) diagram (Le Bas et al., 1986) (Fig. 7a). Melhaq Formation volcanic rocks are basaltic andesite, andesite and dacite, whereas the Heib Formation volcanics are dacite and rhyolite. The calc-alkaline character of these volcanics is shown on the AFM diagram (Fig. 7b) of Irvine and Baragar (1971). When compared to Cryogenian (older metavolcanic "OMV"; younger metavolcanics "YMV") and Ediacaran (Dokhan) volcanic rocks from the Eastern Desert of Egypt and the Sinai Peninsula, Kid Group lavas are remarkably similar to those of the Dokhan Volcanics of NE Desert, Egypt (Fig. 7a, b). The Kid Group volcanic rocks have a wide range of MgO (0.13–5.56 wt.%), CaO (0.25–6.89 wt.%), total iron as Fe_2O_3 (1.55–7.76 wt.%), Al_2O_3 (12.07–17.87 wt.%) and TiO_2 (0.19–1.14 wt.%) contents. Their Na_2O (3.43–5.17 wt.%) and K_2O (1.8–5.9 wt.%) contents are high and variable. The contents of Al_2O_3, MgO, CaO and Fe_2O_3 decrease with increasing SiO_2 in both Melhaq and Heib volcanic rocks, which plot mainly in the fields of Dokhan Volcanics of the Eastern Desert and correlative Ediacaran volcanics in Sinai (Fig. 8a–d). The systematic variation for the major elements could be evidence of fractional crystallization as indicated by the curvilinear trends of some elements, especially MgO. The trends are qualitatively consistent with the fractionation of plagioclase and ferromagnesian minerals as indicated by decreasing MgO and CaO with increasing SiO_2. Heib Formation lavas show decreasing Na_2O with increasing SiO_2 (not shown), suggesting that sodic feldspar was a major fractionating phase.

Kid granites have high SiO_2 (73.9–79.2 wt.%) and Na_2O (3.95–2.75 wt.%) contents with $Na_2O/K_2O<1$. They are mostly syenogranite (Fig. 7c) according to the R1–R2 classification scheme of de la Roche et al. (1980). The Al_2O_3 contents range between 11.18 and 13.04 wt.%,

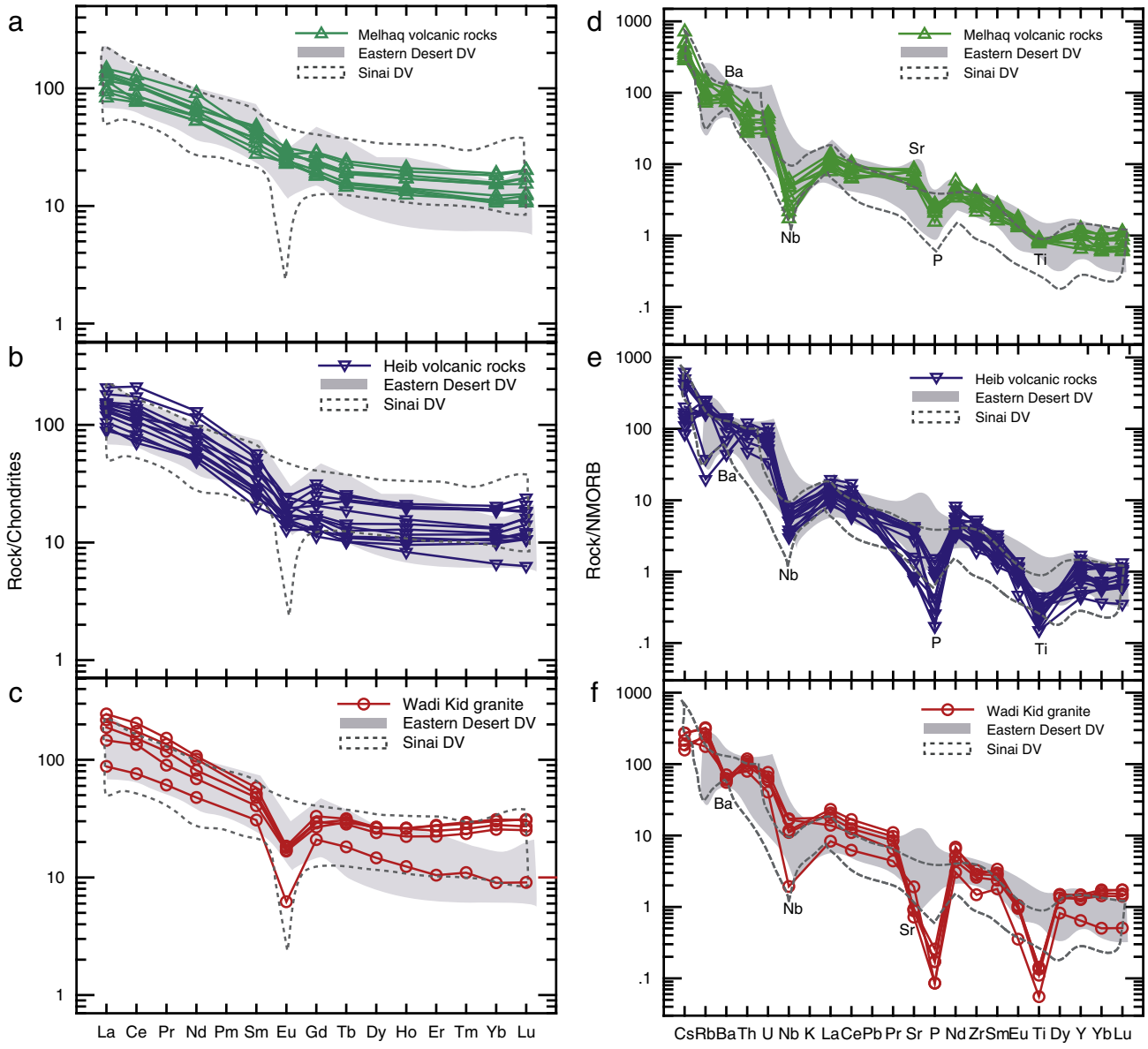

Fig. 9. Chondrite-normalized REE patterns (a, b, c) and MORB-normalized multi-element diagrams (d, e, f) for the Melhaq volcanics, Heib volcanics and Kid granites, respectively, Wadi Kid area, SE Sinai, Egypt. Sinai DV (dashed field) include data for Ediacaran lavas from Rutig (Be'eri-Shlevin et al., 2011), Kid Volcanics (El-Bialy, 2010), and Wadi Rufaiyil (Azer and Farahat, 2011).
Normalizing values of MORB and chondrite are from Sun and McDonough (1989). Gray field is for Dokhan Volcanics in the Eastern Desert of Egypt, with data from Abdel Rahman (1996), Eliwa et al. (2006), Moghazi (2003), and Stern and Gottfried (1986).

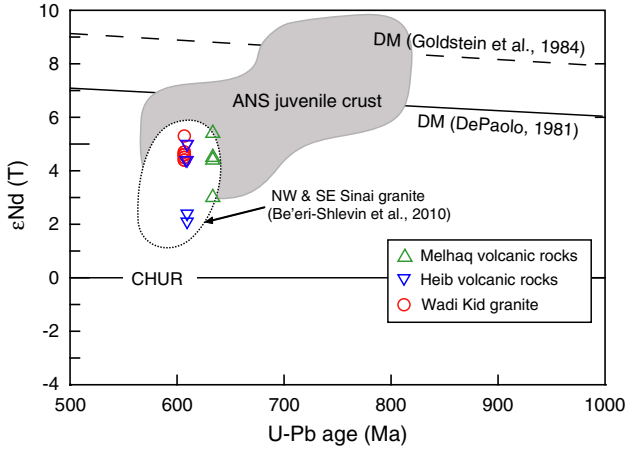

Fig. 10. Plot of εNd(T) versus U–Pb zircon age for the Melhaq and Heib volcanics and post-collisional granites of Wadi Kid, SE Sinai, Egypt.
The reference line for chondritic uniform reservoir (CHUR) and the depleted mantle evolution curves (DM) are from DePaolo (1981) and Goldstein et al. (1984). The data for the field of the Arabian–Nubian Shield (ANS) juvenile crust are from Ali K.A. et al. (2009), Ali et al. (2010), Ali et al. (2012), Claesson et al. (1984), Hargrove et al. (2006), Liégeois and Stern (2010), Moussa et al. (2008), and Stoeser and Frost (2006). The data for the field of NW and SE Sinai granite are from Be'eri-Shlevin et al. (2010).

and the contents of CaO, MgO, TiO_2 and P_2O_5 are low (mean = 0.68, 0.11, 0.15 and 0.02 wt.%, respectively). The modified alkali lime index (MALI) shows their calc-alkaline to alkali-calcic character (Frost et al., 2001) (Fig. 7d). Overall, the chemical compositions are similar to the highly evolved rhyolites of the Heib Formation, which might be extrusive equivalents, linked perhaps via the Kid caldera complex inferred by Azer et al. (2010).

6.3. Trace element variations

In the Kid Group volcanic rocks, large ion lithophile elements (LILE) such as Rb (11–143 ppm), Ba (438–976 ppm) and Sr (74–704 ppm) and high field strength (HFS) elements such as Zr (140–396 ppm), Hf (4.3–9.0 ppm), Nb (4–9 ppm), Y (11–48 ppm), and Ta (0.59–1.32 ppm) show large variations. Cr contents are in the range of 17–140 ppm and Ni contents range from 2 to 87 ppm. The Mg# (= 100 Mg/Mg + Fe) and contents of Cr and Ni in the most primitive samples (samples MV26-2 and MV42-2, Table A1 — supplementary materials) vary between 59 and 67, 63 and 140 ppm and 11 and 87 ppm, respectively, and show that even the most primitive lavas are fractionated relative to primary mantle melts. Selected trace elements for Kid volcanic rocks and granites are plotted against SiO_2 in Fig. 8e–h. These elements show similar concentrations to the Dokhan Volcanics. The variation of large ion lithophile element concentrations (Rb, Ba, Sr) vs. silica confirms the early fractionation of plagioclase (early increase in Ba accompanying decrease in Sr) during the evolution of the Melhaq volcanics and K-feldspar fractionation (rapid decrease of Ba in the rhyolites and granites) during the evolution of the Heib volcanics. The increase in Rb and decrease in Sr also confirm plagioclase fractionation. Ni also correlates negatively with SiO_2.

Chondrite-normalized REE patterns show that the volcanic and granite rocks are variably light-REE enriched according to rock type (Fig. 9a–c). Again, younger Heib Formation lavas are more fractionated than those of the Melhaq Formation. The Melhaq volcanics (andesite and dacites) are characterized by moderate total REEs (104–173 ppm) and moderately fractionated patterns [(La/Yb)n = 6.1–12.4] with weakly negative Eu-anomalies (Eu/Eu^* = 0.7–1.0). The Heib volcanics (dacites and rhyolites) have higher REE contents (100–261 ppm) and show more fractionated REE patterns [(La/Yb)n = 7–13] with weak to moderate negative Eu anomalies (Eu/Eu^* = 0.5–0.9). However, the REE concentrations of the Kid granites are high and variable (∑REE = 113–285 ppm), with less LREE enrichment [(La/Yb)n = 2.9–4.3], and slightly fractionated HREE patterns [(Gd/Yb)n = 0.9–2.3]. Strong negative Eu anomalies [(Eu/Eu^*) = 0.2–0.5] indicate feldspar-controlled. MORB-normalized incompatible element profiles of the volcanic and granitic rocks (Fig. 9d–f) display negative Nb anomalies, evidence that the melt source was modified by subduction-related fluids (Pearce, 1983). The rhyolites and granites have "spikier" multi-element patterns and variably negative Ba, Sr, P, Eu, and Ti anomalies, which may reflect plagioclase, K-feldspar, apatite, and Fe–Ti oxide fractionation. The REE and MORB-normalized trace element patterns of the Kid volcanics are overall similar to those of the Dokhan Volcanics from the Eastern Desert of Egypt and Sinai (Fig. 9).

6.4. Nd isotopes

The εNd(t) values vary from +3.0 to +5.5 for the Melhaq volcanics, from +2.1 to +5.0 for the Heib volcanics, and from +4.6 to +5.4 for the Kid granites. It is evident that regardless of rock type, εNd shows little variation and the vast majority of samples are between +4.4 and +5.5. These data require derivation from a source with a time-integrated depletion in Nd relative to Sm, indicating a strongly depleted, upper-mantle-like chemical reservoir. Three samples (2 Heib, 1 Melhaq) have εNd(t) between +2.1 and +3.0, which are somewhat lower but still consistent with that expected for a depleted mantle source at that time. Nd model ages (T_{DM}) for samples with $^{147}Sm/^{144}Nd \leq 0.165$ are regarded as meaningful (Stern, 2002). All of our samples pass this filter (Table 2) and therefore the T_{DM} model ages are considered reliable. Most of the analyzed samples yield Nd-depleted mantle model ages (T_{DM}, DePaolo, 1981) in the range 0.71–0.88 Ga, which is similar to the mean $T_{DM} = 0.84 \pm 0.10$ Ga for Sinai–Israel–Jordan basement rocks (Stern, 2002). These model ages are also similar to the U–Pb zircon ages determined for the oldest Neoproterozoic Sinai basement (850–780 Ma, Stern and Manton, 1987; Kröner et al., 1990; Eyal et al., 1991) and indicate extraction of juvenile magma from the mantle without significant contribution from long-lived crustal components. However, the three samples that have εNd between +2.1 and +3.0 give T_{DM} model ages of about 1 Ga (Table 2). Similar old T_{DM} ages were also recorded in granites from NW and SE Sinai by Be'eri-Shlevin et al. (2010). Around 1 Ga zircons are increasingly being reported from northern Sinai basement exposures (Be'eri-Shlevin et al., 2009c; Bea et al., 2009), but we encountered no zircons of this age in our study. The εNd(T) results for the studied rocks are plotted against age (Fig. 10). Their isotopic compositions are lower than that of the depleted mantle model of DePaolo (1981) and plot towards the enriched part of the ANS juvenile crust (Liégeois and Stern, 2010; Stern et al., 2010a, 2010b). There is no difference on this diagram (Fig. 8) between our samples and those from NW and SE Sinai (Be'eri-Shlevin et al., 2010), and the overall trend for Neoproterozoic igneous rocks in Sinai may suggest minor crustal contamination. If the magmas represented by these samples experienced a significant contribution of pre-Neoproterozoic crust, the samples would exhibit much lower εNd considering the sensitivity of Nd isotopes to such input (Küster et al., 2008; Liégeois and Stern, 2010; Stern et al., 2010a,2010b).

7. Discussion

Fig. 11 summarizes the reconstructed stratigraphy of the Kid Group according to our field observations and U-Pb ages. The following discussion focuses on 1) Age and provenance of the Um Zariq metasediments; 2) Tectonic setting of the Kid Group; and 3) Petrogenesis of Wadi Kid igneous rocks.

7.1. Age and Provenance of the Um Zariq metasediments

Most U–Pb zircon age data from Sinai suggests early crustal formation between ca. 850 and 740 Ma (Bea et al., 2009, El-Shafei and Kusky, 2003;

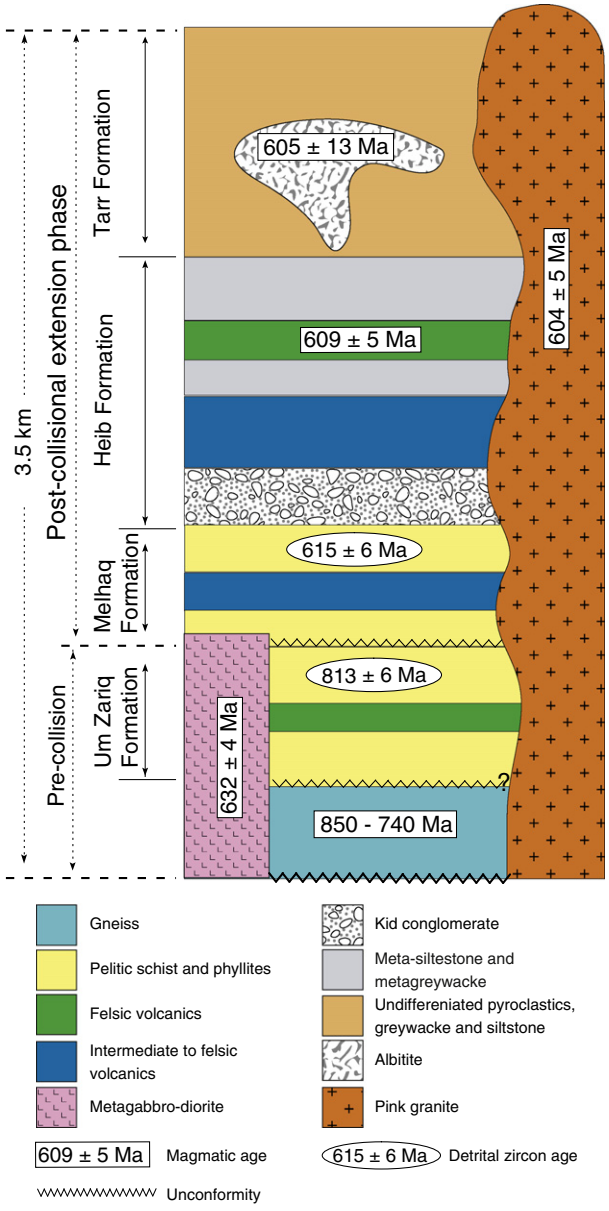

Fig. 11. Diagram showing the stratigraphy and relationships between the different rock units within the Wadi Kid. The U–Pb zircon ages are marked and the tectonic stages of evolution of the entire Kid complex are shown.

Kröner et al., 1990), coeval with estimates for crustal formation in the southern ANS. Scarce inherited zircons pre-dating ca. 870 Ma have been detected in some magmas (Ali B.H. et al., 2009; Be'eri-Shlevin et al., 2009a; Breitkreuz et al., 2010), and similarly old detrital zircons are found in various Neoproterozoic sediments (Be'eri-Shlevin et al., 2009a; Samuel et al., 2011; Stern et al., 2010a,2010b), but actual crust older than 870 Ma is rare in the northernmost ANS (Be'eri-Shlevin et al., 2012). Recently, Be'eri-Shlevin et al. (2012) documented the first evidence of latest Mesoproterozoic (U–Pb zircon ages of ca. 1.03–1.02 Ga) island arc rocks in the Sa'al volcano-sedimentary complex in Sinai (Fig. 1b). We see no evidence of this or any other pre-Neoproterozoic crust in the age distribution patterns of detrital zircons from the Kid Group metasediments that are < 10% discordant as presented in Fig. 5b, c.

The detrital zircon age spectrum of the Um Zariq Formation is significantly different from that of the Melhaq Formation. Most Um Zariq Formation ages cluster between 800 Ma and 830 Ma (peak at 813 Ma); smaller age clusters occur at 891, 763 and 647 Ma with a clear gap in ages between 763 Ma and 647 Ma (Fig. 5b). The Um Zariq metasedimentary rocks could thus have been derived from Cryogenian ANS crust in the region (650–870 Ma). The detrital zircon ages also indicate ~890 Ma rocks in the source of Um Zariq metasediments. This source is not common in northernmost ANS, as the oldest dated magmatic rocks in Sinai are the ca. 844 Ma Muneiga quartz diorite (Bea et al., 2009) and the ca. 1.03–1.02 Ga Sa'al volcano-sedimentary complex (Be'eri-Shlevin et al., 2012). Detrital zircons of ca. 900–1100 Ma, dominated by a population at ca. 960 Ma, are also recorded in sediments from southern Sinai (Samuel et al., 2011). This suggests that pre-870 Ma components of dominantly latest Mesoproterozoic to earliest Neoproterozoic age were more widespread in the northern ANS than previously thought. Zircons in Melhaq metasediment sample range between ca. 615 Ma and 808 Ma; however, several age clusters are evident. Most grains fall into the population ~615 Ma, but there are three minor age groups at 715, 777 and 808 Ma. The combined age range (i.e. 615–808 Ma) is similar to that of known ANS components.

The contrast in detrital zircon populations between the Um Zariq and Melhaq metasediments can be interpreted as follows: (a) abundant Cryogenian ages (750–891 Ma) in the Um Zariq metasediments suggest that crust of this age was dominant within the drainage basin during deposition of Um Zariq Formation. Alternatively, Um Zariq metasediments may be Cryogenian, deposited much earlier than the other Kid Group sequences; (b) considering the vast amount of uplift and erosion that characterized the northernmost ANS after ca. 635 Ma (Avigad and Gvirtzman, 2009; Be'eri-Shlevin et al., 2009a; Blasband et al., 1997; Garfunkel, 1999), the Melhaq sediments may have been deposited in a deep marine basin for which Ediacaran volcanics were the main source and old Neoproterozoic crust did not exist or was buried.

7.2. Tectonic setting of the Ediacaran Kid Group

The tectonic setting where the Ediacaran Kid Group formed is debated. The Melhaq and Um Zariq formations have been described as marine sediments of back-arc ophiolite affinity (Shimron, 1981, 1983), or simply back-arc/arc-related calc-alkaline volcanics and sediments (Abu El-Enen, 2008; Furnes et al., 1985; Ghoneim et al., 1985), but in fact the Um Zariq sediments differ fundamentally from other Ediacaran sequences in the area. An alternative view is that the Melhaq–Heib–Tarr volcanics and sediments are equivalent to Dokhan Volcanics and Hammamat Group sediments of the Eastern Desert (El-Bialy, 2010; El-Gaby et al., 1991; El-Metwally et al., 1999; Hassanen, 1992). Heib volcanic rocks have been interpreted as active continental margin (Andean) eruptives (El-Gaby et al., 1991; Furnes et al., 1985; Shimron, 1984), whereas the Tarr Complex was interpreted by Shimron (1983, 1984) as forming in a fore-arc accretionary prism. On the other hand, more recent studies interpret the Kid Group as having formed in an extensional tectonic setting (Blasband et al., 1997, 2000; Brooijmans et al., 2003). Recently, Fowler et al. (2010a, b) inferred compressional deformation and a thrust origin for deformation of the Kid complex. They suggested a model that involved an active continental margin that was deformed by collision and compression in a NW–SE to N–S to NNE–SSW direction through most of its history. These collisional deformation events were interpreted to have occurred between 650 and 620 Ma, i.e., before regional extension began about 610 Ma (Fowler and El-Kalioubi, 2004; Fowler and Osman, 2009; Greiling et al., 1994). The reasons for such debate on the paleotectonic environment of the Kid Group can be attributed to the confusion about when subduction stopped beneath the northern ANS (Be'eri-Shlevin et al., 2009b) and to the complicated deformation history of the Wadi Kid area (Blasband et al., 1997).

The Um Zariq Formation is commonly carbonaceous and has aluminous phases such as cordierite, garnet, staurolite and andalusite indicating that it was originally mostly aluminous shale. Its age (probably Cryogenian) and lithology are fundamentally different from the rest of

the Kid Group (Melhaq, Heib and Tarr formations) that comprise early Ediacaran (615–604 Ma) volcanic rocks interbedded with immature sediments including conglomerates, sandstones and siltstones. Thus, the Um Zariq sediments may be older and reflect a deposition period without significant volcanic activity. On the other hand, the early Ediacaran Melhaq, Heib and Tarr volcano-sedimentary formations likely evolved within relatively small basins, as inferred from the association with conglomerates and other immature sediments. The early Ediacaran in the northernmost ANS was characterized by extensive development of volcano-sedimentary successions in isolated basins. In Sinai, the volcano-sedimentary successions from the Rutig and Ferani areas (high-K calcalkaline intermediate to silicic volcanics, interbedded with immature sediments) display marked similarities to the Kid succession in terms of the lithologies and ages of both volcanics and associated sediments (Be'eri-Shlevin et al., 2011; El-Gaby et al., 1991, 2002; Moussa, 2003; Samuel et al., 2011). Dacites and rhyolites from Rutig and Ferani volcanic successions yield ages between ca. 627 and 593 Ma (Be'eri-Shlevin et al., 2011), similar to the U–Pb zircon ages of 630–590 Ma reported for the Dokhan volcanics–Hammamat sediments in the Eastern Desert of Egypt (Breitkreuz et al., 2010; Wilde and Youssef, 2000), which is very close to that of the Wadi Kid volcano-sedimentary rocks.

To the east and west of Sinai ca. 600–590 Ma immature sediments have been identified in southern Israel (Elat conglomerate, Garfunkel, 1999), southwestern Jordan (Saramuj conglomerate, Jarrar et al., 1993, 2003), the Midyan terrane of northwest Saudi Arabia (Minawa Formation, Clark, 1985) and in the ED of Egypt (Hammamat clastics, Breitkreuz et al., 2010; Wilde and Youssef, 2000, 2002; Willis et al., 1988). Our new U–Pb age results show that the Melhaq, Heib and Tarr successions and the Kid granites (615–604 Ma) evolved coevally with the Dokhan–Hammamat volcano-sedimentary succession and the Younger Granites in the northern ANS.

Similar Early Ediacaran volcano-sedimentary units exist in Jordan (e.g., >595 Ma Saramuj Conglomerate; Jarrar et al., 1993). New, unpublished U–Pb zircon ages suggest that the 600–610 Ma Haiyala Volcaniclstic Formation and 598 Ma Aheimir rhyolites (Jarrar, pers. comm. 2012) may also correlate with the NED and Sinai Dokhan–Hammamat sequences, in which case a huge, largely felsic volcanic field can be envisioned covering the region, laced with rivers that carried detritus from volcanoes to intervening rift basins.

Geochemically, both intermediate and silicic magmas of the Melhaq, Heib and Tarr successions are similar to the Dokhan Volcanics of the Eastern Desert of Egypt and Sinai (Figs. 7 and 8). Moreover, they all show similar MORB trace element and chondrite normalized REE patterns (Fig. 9).

Several authors have suggested that these units were emplaced during post-collision extensional collapse that followed continental collision during late-stages of the Neoproterozoic crustal evolution (Avigad and Gvirtzman, 2009; El-Bialy, 2010; Eyal et al., 2010; Moghazi, 2003). Blasband et al. (1997, 2000) noted extensional structures in the Kid area including a metamorphic core complex and detachment faults and suggested that the region experienced extensional collapse. According to our field observations, the Kid metamorphic core complex and detachment were active prior to the intrusion of the Kid granites (604 Ma, this study). This is because this intrusion neither intrudes extensional structures nor is bounded by low-angle normal faults (Avigad and Gvirtzman, 2009). Therefore, deformation in the Kid area was over by the time the undeformed Kid Granite (604±5 Ma) and Tarr albitite–carbonatite complex (605±13 Ma) was intruded. Deformation affected Melhaq Formation sediments, which were deposited some time after ~615 Ma, and the 609±5 Ma Heib Formation rhyolites, indicating that deformation was stopped by ~610 Ma.

7.3. Petrogenesis of magmas in the Kid area

7.3.1. Fractional crystallization/crustal contamination

Rocks representing primary melts in equilibrium with mantle peridotite should have Mg# >65 and 200–450 ppm Ni (Frey et al., 1978). In the Kid volcanic rocks, even the most mafic samples (~55 wt.% SiO_2) are not primary because Ni contents are too low (11–87 ppm, Table 1) and are likely the products of fractional crystallization of olivine and clinopyroxene as evidenced by negative correlations between SiO_2 vs. MgO, Al_2O_3, and CaO (Fig. 6). The presence of negative P and Ti anomalies and their systematic deepening from the intermediate Melhaq volcanic rocks to the Kid granites (Fig. 7d–f) indicate fractionation of apatite and Fe–Ti oxides during magma evolution. Plagioclase fractionation may also have occurred as indicated by increasingly negative Eu anomalies (Fig. 7a–c) and decreasing Sr with increasing SiO_2 (Fig. 6f) from the intermediate to the felsic rocks. The strong depletion of Ba and Sr in the rhyolites and granite (strong negative anomalies; Fig. 7e, f) indicates K-feldspar fractionation as well as plagioclase.

Significant contamination of pre-Neoproterozoic crust can be excluded based on the positive εNd(t) values (+2.1 to +5.5) and Sr_i values (0.7022 to 0.7030) of the samples, which are similar to those of Neoproterozoic juvenile ANS crust. However, the presence of Cryogenian xenocrystic zircons (~800 Ma; Fig. 3e) in the rhyolite along with

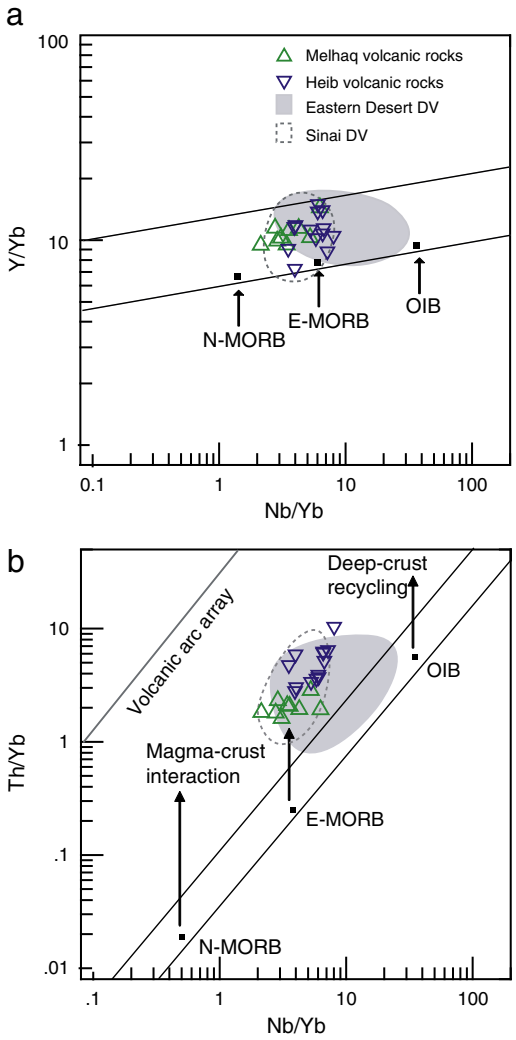

Fig. 12. (a) Y/Yb vs. Nb/Yb diagram for the Kid and Heib volcanic rocks, SE Sinai, Egypt, showing that the least evolved samples plot in the mantle array, (b) Th/Yb vs. Nb/Yb diagram showing the least evolved samples displaced from the MORB–OIB array and illustrating the influence of subduction fluid. MORB and OIB represent the composition of the mid-ocean ridge and oceanic island mantle source, respectively.
The mantle array (MORB–OIB) is after Green (2006) and Pearce (1983). Gray field is for the Dokhan Volcanics in the Eastern Desert and the dashed field if for Dokhan Volcanics from Sinai, with data from Abdel Rahman (1996), Azer and Farahat (2011), Be'eri-Shlevin et al. (2011), Eliwa et al. (2006), El-Bialy (2010), Moghazi (2003), and Stern and Gottfried (1986).

variation in the εNd(t) values may suggest minor contamination with pre-existing Cryogenian crust.

7.3.2. Magma source

The calc-alkaline characteristics, including marked enrichments in LILE and LREE and depletions in Nb–Ta, of the least evolved volcanic rocks from the Melhaq Formation were likely inherited from a mantle source that had been metasomatized by melts/fluids released from a subducting slab (e.g., Gertisser and Keller, 2003; Kogiso et al., 2009; Turner et al., 1992), or modified by subducted sediments and associated fluids/melts (e.g., Plank, 2005; Plank and Langmuir, 1998; Stolz et al., 1988, 1990; Woodhead et al., 1998) and not the result of crustal contamination. HFSE behave in a conservative way during subduction, so their concentration in the rocks reflects that in the mantle wedge. LILE and LREE, on the other hand, are non-conservative elements and their concentration in the rocks can be used to evaluate the slab contribution to the mantle wedge (Pearce, 2008; Pearce and Peate, 1995). Thus, Y/Yb and Th/Yb vs. Nb/Yb plots (Pearce, 1983; Pearce and Peate, 1995) can be used to evaluate the mantle and slab contribution to the magma. On these discrimination diagrams (Fig. 12; Pearce, 1983), MORB and uncontaminated intra-plate basalts (OIB) plot in a well-defined array with a slope of unity, indicating that mantle enrichment events appear to equally concentrate Nb, Y and Th (Wilson, 1989). On the Y/Yb vs. Nb/Yb diagram (Fig. 12a), the least evolved Melhaq volcanic rocks plot within the mantle array close to E-MORB indicating derivation from a mantle source. In contrast, on the Th/Yb vs. Nb/Yb (Fig. 12b), the rocks are displaced towards higher Th/Yb due to the influence of subduction zone fluids enriched in Th.

In general, metasomatism related to fluids/melts released from a subducting oceanic slab increases Ba/Th but does not change the Nd isotopic composition of the mantle source, which commonly has high εNd(t) (e.g., Gertisser and Keller, 2003; Guo et al., 2005; Peng et al., 2008; Shimoda et al., 1998). Thus, the slightly low εNd(t) (+2.1 to +5.5) of Melhaq Formation volcanic rocks compared to that expected for depleted mantle at the time of their formation likely resulted from modification of the upper mantle by subducted sediments. Moreover, arc-like high-Al volcanic rocks generally have higher Th/Ce, Nb/Zr and Th/Nb ratios than those of MORB-sourced volcanic rocks, and are commonly interpreted as the result of the input of sediments into their mantle source (e.g., Gertisser and Keller, 2003; Kimura and Yoshida, 2006; Petrone et al., 2003; Seghedi et al., 2001, 2004). The least evolved samples (MV42-2 and MV26-2, Table A2 — supplementary materials) of the Melhaq volcanic rocks contain more Al_2O_3 (16.6–17.9 wt.%), and have higher Th/Ce (0.08–0.09) and Th/Nb (0.52–0.80) ratios compared to those of MORB (0.02 and 0.065, respectively), suggesting the involvement of subducted sedimentary materials in their magma source (e.g., Plank and Langmuir, 1998; Stolz et al., 1988, 1990).

In the northern ANS, post-collisional rocks with these features are considered to represent derivation of magmas from a lithospheric mantle which has been previously metasomatized by earlier subduction-related processes (e.g. El-Bialy, 2010; Eyal et al., 2010; Friz-Topfer, 1991; Iacumin et al., 1998; Kessel et al., 1998; Moghazi, 2003) or from melting of subducted oceanic crust (e.g., Bogoch et al., 2003; Eliwa et al., 2006; Katz et al., 2004). However, Be'eri-Shlevin et al. (2009a, b, 2011) pointed out that continental collision in the northernmost ANS likely involved few fragments of oceanic crust during its late stages (ca. 635–620 Ma), which does not support the model of melting subducted oceanic crust. Thus, the most likely source of Kid volcanics and granites is a lithospheric mantle that has been previously metasomatized by earlier subduction-related processes. This can be viewed within a model of extensional collapse that follows continental collision and controlled mainly by lithospheric delamination and/or slab breakoff. In this model (Davies and von Blanckenburg, 1995), slab breakoff and lithospheric delamination lead to upwelling of the hot asthenosphere that impinges on the base of mantle lithosphere causing it to partial melt and produce enriched magmas. The lithospheric mantle involved has unique trace element characteristics owing to its interaction with fluids and melts driven off from the subducting slab during Cryogenian subduction (i.e. between 850 and 620 Ma; Stern, 1994) to form the Arabian–Nubian Shield.

8. Conclusions

Geochronological and geochemical data (including Sr–Nd isotopes) for the Wadi Kid volcano-sedimentary succession and granites in southeastern Sinai allow us to reach the following conclusions:

(1) The Kid Group includes the Um Zariq Formation (metapelites and metapsammites interbedded with metagreywackes and metatuffs), Melhaq Formation (calc-alkaline meta-andesites and metadacites interbedded with immature sediments), Heib and Tarr Formations (dominated by highly fractionated dacites and rhyolites and interbedded with weakly metamorphosed immature sediments of siltstone, sandstone and conglomerate). All formations are intruded by alkali granites and locally albitite.

(2) U–Pb ages of detrital zircons from the Um Zariq Formation are as young as 647 ± 12 Ma, but 19 concordant zircons give an age of 813 ± 6 Ma, which may be close to the maximum depositional age of this unit. The Um Zariq metasediments are potentially older than other Cryogenian formations in the area, and may reflect deposition in the absence of significant volcanic activity.

(3) The Melhaq, Heib and Tarr formations record several phases of Ediacaran (615–607 Ma) sedimentation and volcanic activity and associated alkali granite and albitite (605–602 Ma) intrusions. The age probability patterns of Melhaq metasediments reveal a zircon age peak at 615 Ma that signifies deposition of immature sediments within isolated basins.

(4) The Melhaq, Heib and Tarr formations and the Kid granites compare well in terms of age, lithology and geochemical patterns with the Dokhan Volcanics–Hammamat sediments and Younger Granites of the Eastern Desert of Egypt. We interpret magmatic activity in the Kid area to have occurred in a similar post-collisional tectonic regime.

(5) The post-collisional Kid volcanic rocks are characterized by continuous variation trends in major and trace elements similar to those expected from fractional crystallization of a single magma. Their calc-alkaline to alkali-calcic characteristics, marked enrichments in LILE and LREE and depletions in Nb–Ta, are likely inherited from a mantle source that had been metasomatized by melts/fluids released during subduction. The absence of pre-Neoproterozoic zircons and the positive εNd(t) values (+2.1 to +5.5) for the volcanic and granitic rocks indicates magma derivation from a juvenile source, with no evidence of older continental crust.

(6) A model of extensional collapse following East and West Gondwana collision, and controlled mainly by lithospheric delamination and slab breakoff, is suggested for the origin of the Kid volcanic rocks and granites. Major asthenospheric upwelling heated the lithospheric mantle and triggered the vast plutonic and volcanic activity.

Supplementary data to this article can be found online at http://dx.doi.org/10.1016/j.lithos.2012.07.003.

Acknowledgments

The authors would like to thank the Institute of Geology and Geophysics, Chinese Academy of Sciences, Beijing for performing the U–Pb isotope analyses. We also thank the Mineralogical–Geological Museum at the University of Oslo for help with the geochemical and isotopic analyses. We are grateful to Dr. J.P. Liégeois, Prof. Mokhles Azer, and Editor-in-Chief Prof. Nelson Eby for critical reviews that improved this manuscript. This is UTD Geosciences contribution number #1233 and TIGeR publication #421. This is also a JEBEL contribution.

References

Abdel Rahman, A.M., 1996. Pan-African volcanism: petrology and geochemistry of Dokhan Volcanic suite in the northern Nubian Shield. Geological Magazine 133, 17–31.

Abdelsalam, M.G., Liégeois, J.P., Stern, R.J., 2002. The Saharan metacraton. Journal of African Earth Sciences 34, 119–136.

Abu El-Enen, M.M., 2008. Geochemistry and metamorphism of the Pan-African back-arc Malhaq volcano-sedimentary Neoproterozoic association, W. Kid area, SE Sinai, Egypt. Journal of African Earth Sciences 51, 189–206.

Abu El-Enen, M.M., 2011. Geochemistry, provenance, and metamorphic evolution of Gabal Samra Neoproterozoic metapelites, Sinai, Egypt. Journal of African Earth Sciences 59, 269–282.

Abu El-Enen, M.M., Zalata, A.A., El-Metwally, A.A., Okrusch, M., 1999. Orthogneisses from the Taba metamorphic belt, SE Sinai, Egypt: witnesses for granitoid magmatism at an active continental margin. Neues Jahrbuch Mineralogie Abhandlungen 175, 53–81.

Abu El-Enen, M.A., Okrusch, M., Will, T.M., 2003a. The metamorphic evolution of the Pan-African basement in the Sinai Peninsula, Egypt. In: Fifth International Conference on the Geology of the Middle East, Cairo, Egypt, pp. 207–216.

Abu El-Enen, M.M., Okrusch, M., Will, T.M., 2003b. Metapelitic assemblages in the Umm Zariq schists, central western Kid Belt, Sinai Peninsula, Egypt. Neues Jahrbuch für Mineralogie — Abhandlungen 178, 277–306.

Abu El-Enen, M.M., Okrusch, M., Will, T.M., 2004. P–T evolution of the Taba Metamorphic belt, Egypt: constraints from the metapelite assemblages. Journal of African Earth Sciences 38, 59–78.

Abu-Alam, T.S., Stuwe, K., 2009. Exhumation during oblique transpression: The Feiran–Solaf region, Egypt. Journal of Metamorphic Geology 27, 439–459.

Akaad, M.K., Noweir, A.M., 1969. Lithostratigraphy of Hammamat-Um Seleimat district, Eastern Desert Egypt. Nature 223, 284–285, http://dx.doi.org/10.1038/223284a0.

Ali, B.H., Wilde, S.A., Gabr, M.M.A., 2009a. Granitoid evolution in Sinai, Egypt, based on precise SHRIMP U–Pb ziron geochronology. Gondwana Research 15, 38–48.

Ali, K.A., Stern, R.J., Manton, W.I., Kimura, J.-I., Khamees, H.A., 2009b. Geochemistry, Nd isotopes and U–Pb SHRIMP zircon dating of Neoproterozoic volcanic rocks from the Central Eastern Desert of Egypt: new insights into the 750 Ma crust-forming event. Precambrian Research 171, 1–22.

Ali, K.A., Stern, R.J., Manton, W.I., Kimura, J.-I., Whitehouse, M.J., Mukherjee, S.K., Johnson, P.R., Griffin, W.R., 2010. Geochemical, U–Pb zircon and Nd isotope investigations of the Neoproterozoic Ghawjah Metavolcanic rocks, Northwestern Saudi Arabia. Lithos 120, 379–393.

Ali, K.A., Moghazi, A.M., Maurice, A.E., Omar, S.A., Wang, Q., Wilde, S.A., Moussa, E.M., Manton, W.I., Stern, R.J., 2012. U–Pb zircon dating, geochemistry, and Sm–Nd isotopic composition of A-Type granites from Humr Akarim and Humrat Mukbid, Eastern Desert, Egypt: no evidence of pre-Neoproterozoic crust. International Journal of Geosciences, http://dx.doi.org/10.1007/s00531-012-0759-2.

Allégre, C.J., Hart, S.R., Minster, J.F., 1983. Chemical structure and evolution of the mantle and continents determined by inversion of Nd and Sr isotopic data, II. Numerical experiments and discussions. Earth and Planetary Science Letters 37, 191–213.

Atalla, R.F., 1989. Geology and metamorphic history of Kid area, southeastern Sinai, Egypt. Unpublished Ph.D. Thesis, Assiut University, Egypt, 174 pp.

Avigad, D., Gvirtzman, Z., 2009. Late Neoproterozoic rise and fall of the northern Arabian–Nubian shield: the role of lithospheric mantle delamination and subsequent thermal subsidence. Tectonophysics 477, 217–228.

Avigad, D., Sandler, A., Kolodner, K., Stern, R.J., McWilliams, M., Miller, N., Beyth, M., 2005. Mass-production of Cambro–Ordovician quartz-rich sandstone as a consequence of chemical weathering of Pan-African terranes: environmental Implications. Earth and Planetary Science Letters 240, 818–826.

Azer, M.K., 2007. Tectonic significance of Late Precambrian calc-alkaline and alkaline magmatism in Saint Katherina area, South Sinai, Egypt. Geologica Acta 5 (3), 255–272.

Azer, M.K., Farahat, E.S., 2011. Late Neoproterozoic volcano-sedimentary successions of Wadi Rufaiyil, southern Sinai, Egypt: a case of transition from late to post-collisional magmatism. Journal of Asian Earth Sciences 42, 1187–1203.

Azer, M.K., Stern, R.J., Kimura, J.-I., 2010. Origin of a Late Neoproterozoic (605 ± 13 Ma) intrusive carbonate–albitite complex in Southern Sinai, Egypt. International Journal of Earth Sciences 99, 245–267.

Basta, E.Z., Kotb, H., Awadalla, M.F., 1980. Petrochemical and geochemical characteristics of the Dokhan Formation at the type locality, Jabal Dokhan, Eastern Desert, Egypt. Institute of Applied Geology of Jeddah Bulletin 3, 121–140.

Be'eri-Shlevin, Y., Katzir, Y., Valley, J.W., 2009a. Crustal evolution and recycling in a juvenile continent: oxygen isotope ratio of zircon in the northern Arabian Nubian Shield. Lithos 107, 169–184.

Be'eri-Shlevin, Y., Katzir, Y., Whitehouse, M., 2009b. Post-collisional tectonomagmatic evolution in the northern Arabian–Nubian Shield (ANS): time constraints from ion-probe U–Pb dating of zircon. Journal of the Geological Society of London 166, 71–85.

Be'eri-Shlevin, Y., Katzir, Y., Whitehouse, M.J., Kleinhanns, I.C., 2009c. Contribution of pre Pan-African crust to formation of the Arabian Nubian Shield: new secondary ionization mass spectrometry U–Pb and O studies of zircon. Geology 37, 899–902.

Be'eri-Shlevin, Y., Katzir, Y., Blichert-Toft, J., Kleinhanns, I.C., Whitehouse, M., 2010. Nd–Sr–Hf–O isotope provinciality in the northernmost Arabian–Nubian Shield: implications for crustal evolution. Contributions to Mineralogy and Petrology 160, 181–201.

Be'eri-Shlevin, Y., Samuel, M.D., Azer, M.K., Rämö, O.T., Whitehouse, M.J., Moussa, H.E., 2011. The Ediacaran Ferani and Rutig volcano-sedimentary successions of the northernmost Arabian–Nubian Shield (ANS): New insights from zircon U–Pb geochronology, geochemistry and O–Nd isotope ratios. Precambrian Research 188, 21–44.

Bea, F., Abu-Anbar, M., Monteroa, P., Peresc, P., Talaveraa, C., 2009. The 844 Ma Moneiga quartz-diorites of the Sinai, Egypt: evidence for Andean-type arc or rift-related magmatism in the Arabian–Nubian Shield? Precambrian Research 175, 161–168.

Be'eri-Shlevin, Y., Eyal, M., Eyal, Y., Whitehouse, M.J., Litvinovsky, B., 2012. The Sa'al volcano-sedimentary complex (Sinai, Egypt): a latest Mesoproterozoic volcanic arc in the northern Arabian Nubian Shield. Geology 40, 403–406.

Bentor, Y.K., 1985. The crustal evolution of the Arabo-Nubian massif with special reference to the Sinai Peninsula. Precambrian Research 28, 1–74.

Bentor, Y.K., Eyal, M., 1987. The geology of southern Sinai; its implication for the evolution of the Arabo-Nubian massif. Jebel Sabbagh Sheet. : The Israel Academy of Sciences and Humanities, vol. 1. 484 pp.

Beyth, M., Grunhagen, H., Zilberfarb, A., 1978. An ultramafic rock in the Precambrian of eastern Sinai. Geological Magazine 115, 373–378.

Beyth, M., Stern, R.J., Altherr, R., Kroner, A., 1994. The Late Precambrian Timna igneous complex. Southern Israel—evidence for comagmatic-type sanukitoid monzodiorite and alkali granite magma. Lithos 31 (3–4), 103–124.

Bielski, M., 1982. Stages in the evolution of the Sinai Peninsula. Unpublished Ph.D. Thesis, The Hebrew University of Jerusalem.

Bielski, M., Jager, E., Steinitz, G., 1979. The geochronology of Iqna granite (Wadi Kid Pluton), southern Sinai. Contributions to Mineralogy and Petrology 70, 159–165.

Black, L.P., Kamo, S.L., Allen, C.M., Davis, D.W., Aleinikoff, J.N., Valley, J.W., Mundil, R., Campbell, I.H., Korsch, R.J., Williams, I.S., Foudoulis, C., 2004. Improved $^{206}Pb/^{238}U$ microprobe geochronology by the monitoring of a trace-element-related matrix effect; SHRIMP, ID-TIMS, ELA-ICP-MS and oxygen isotope documentation for a series of zircon standards. Chemical Geology 205 (1–2), 115–140.

Blasband, B., 1995. Structural Geology and Tectonics of Precambrian Metamorphic Rocks in the Sinai, Egypt. MSc Thesis, Utrecht University.

Blasband, B., Brooijmans, P., Dirks, P., Visser, W., White, S., 1997. A Pan-African core complex in the Sinai, Egypt. Geologie en Mijnbouw 76, 247–266.

Blasband, B., White, S.H., Brooijmans, P., de Boorder, H., Visser, W., 2000. Late Proterozoic extensional collapse in the Arabian–Nubian Shield. Journal of the Geological Society of London 157, 615–628.

Blasy, M., El-Baroudy, A.F., Kharbish, S.M., 2001. Geochemical characteristics of Wadi Tarr albitite, southeastern Sinai, Egypt. Egyptian Journal of Geology 45, 767–780.

Bogoch, R., Avigad, D., Weissbrod, T., 2003. Geochemistry of the quartz diorite granite association, Roded area, southern Israel. Journal of African Earth Sciences 35, 51–60.

Breitkreuz, C., Eliwa, H., Khalaf, I., El Gameel, K., Buhler, B., Sergeev, S., Larionov, A., Murata, M., 2010. Neoproterozoic SHRIMP U–Pb zircon ages of silica-rich Dokhan Volcanics in the North Eastern Desert, Egypt. Precambrian Research 182, 163–174.

Brooijmans, P., 1996. Geothermobarometry of a Metamorphic Core Complex, SE Sinai, Egypt. PhD Thesis, Utrecht University.

Brooijmans, P., Blasband, B., White, S.H., Visser, W.J., Dirks, P., 2003. Geothermobarometric evidence for a metamorphic core complex in Sinai, Egypt. Precambrian Research 123, 249–268.

Claesson, S., Pallister, J.S., Tatsumoto, M., 1984. Samarium–neodymium data on two late Neoproterozic ophiolites of Saudi Arabia and implications for crustal and mantle evolution. Contributions to Mineralogy and Petrology 85, 244–252.

Clark, M.D., 1985. Late Proterozoic crustal evolution of the Midyan region, northwestern Saudi Arabia. Geology 13, 611–615.

Compston, W., Williams, I.S., Kirschvink, J.L., Zhang, M.G., 1992. Zircon U–Pb ages for the early Cambrian time-scale. Journal of the Geological Society of London 149, 171–184.

Corfu, F., Hancher, J.M., Hoskin, P.W., Kinny, P., 2003. Atlas of zircon textures. Reviews in Mineralogical and Geochemistry 53, 469–500.

Davies, J.H., Von Blanckenburg, F., 1995. Slab breakoff: a model of lithosphere detachment and its test in the magmatism and deformation of collisional orogens. Earth and Planetary Science Letters 129, 85–102.

de la Roche, H., Leterrier, J., Grandclaude, P., Marchal, M., 1980. A classification of volcanic and plutonic rocks using R1R2 diagram and major-element analyses — its relationships with current nomenclature. Chemical Geology 29, 183–210.

DePaolo, D.J., 1981. Neodymium isotopes in the Colorado Front Range and crust mantle evolution in the Proterozoic. Nature 291, 193–196.

El-Bialy, M.Z., 2010. On the Pan-African transition of the Arabian–Nubian Shield from compression to extension: the post-collision Dokhan volcanic suite of Kid-Malhak region, Sinai, Egypt. Gondwana Research 17, 26–43.

El-Gaby, S., List, F.K., Tehrani, R., 1990. The basement complex of the Eastern Desert and Sinai. In: Said, R. (Ed.), The Geology of Egypt. Balkema, Rotterdam, pp. 175–184.

El-Gaby, S., Khudier, A.A., Abdel Tawab, M., Atalla, R.F., 1991. The metamorphosed volcano-sedimentary succession of Wadi El Kid, South Eastern Sinai, Egypt. Annual Geological Survey, Egypt, 17, pp. 19–35.

El-Gaby, S., Khalaf, I.M., Eliwa, H.A., El-Miligy, A., Gomaa, R.M., 2002. The volcanosedimentary successions of the Wadi Sa'al-Wadi Zaghra area, Southeastern Sinai, Egypt. In: 6th International Conference on Geological Arab World, Cairo University, Egypt, Vol. 1, pp. 25–44.

Eliwa, H.A., Abu El-Enen, M.M., Khalaf, I.M., Itaya, T., 2004. Metamorphic evolution of Sinai metapelites and gneisses: constraints from petrology and K/Ar dating. Egyptian Journal of Geology 48, 169–185.

Eliwa, H.A., Kimura, J.I., Itaya, T., 2006. Late Neoproterozoic Dokhan Volcanics, North Eastern Desert, Egypt: geochemistry and petrogenesis. Precambrian Research 151, 31–52.

Eliwa, H.A., Abu El-Enen, M.M., Khalaf, I.M., Itaya, T., Murata, M., 2008. Metamorphic evolution of Neoproterozoic metapelites and gneisses in the Sinai, Egypt: insights from petrology, mineral chemistry and K–Ar age dating. Journal of African Earth Sciences 51, 107–122.

El-Metwally, A.A., El-Aasy, I.E., Ibrahim, M.E., Essawy, M.A., El-Mowafy, A.A., 1999. Petrological, structural and geochemical studies on the basement rocks of Gabal Um Zariq-Wadi Kid area, South-eastern Sinai. Egyptian Journal of Geology 43, 147–180.

El-Shafei, M.K., Kusky, T.M., 2003. Structural and tectonic evolution of the Neoproterozoic Feiran–Solaf metamorphic belt Sinai Peninsula: implications for the closure of the Mozambique Ocean. Precambrian Research 123, 269–293.

Eyal, M., Bartov, Y., Shimron, A.E., Bentor, Y.K., 1980. Sinai geological map, aeromagnetic map. Survey of Israel, Scale: 1:500 000, 1 sheet.
Eyal, Y., Eyal, M., Kröner, A., 1991. Geochronology of the Elat Terrain, metamorphic basement, and its implications for crustal evolution of the NE part of the Arabian–Nubian Shield. Israel Journal of Earth Sciences 40, 5–16.
Eyal, M., Litvinovsky, B., Jahn, B.M., Zanvilevich, A., Katzir, Y., 2010. Origin and evolution of post-collisional magmatism: coeval Neoproterozoic calc-alkaline and alkaline suites of the Sinai Peninsula. Chemical Geology 269, 153–179.
Fowler, A., El-Kalioubi, B., 2004. Gravitational collapse origin of shear zones, foliations and linear structures in the Neoproterozoic cover nappes, Eastern Desert, Egypt. Journal of African Earth Sciences 38, 23–40.
Fowler, A., Osman, A.F., 2009. The Sha'it–Nugrus shear zone separating Central and South Eastern Deserts, Egypt: a post-arc collision low-angle normal ductile shear zone. Journal of African Earth Sciences 53, 16–32.
Fowler, A., Hassen, I.S., Osman, A.F., 2010a. Neoproterozoic structural evolution of SE Sinai, Egypt: I. Re-investigation of the structures and deformation kinematics of the Um Zariq and Malhaq Formations, northern Wadi Kid area. Journal of African Earth Sciences 58, 507–525.
Fowler, A., Hassen, I.S., Osman, A.F., 2010b. Neoproterozoic structural evolution of SE Sinai, Egypt: II. Convergent tectonic history of the continental arc Kid Group. Journal of African Earth Sciences 58, 526–546.
Frey, F.A., Green, D.H., Roy, S.D., 1978. Integrated models of basalt petrogenesis: a study of quartz tholeiites to olivine melilitites from south-eastern Australia utilizing geochemical and experimental petrological data. Journal of Petrology 19, 463–513.
Friz-Topfer, A., 1991. Geochemical characterization of Pan-African dyke swarms in southern Sinai: from continental margin to intraplate magmatism. Precambrian Research 49, 281–300.
Frost, B.R., Arculus, R.J., Barnes, C.G., Collins, W.J., Ellis, D.J., Frost, C.D., 2001. A geochemical classification of granitic rocks. Journal of Petrology 42, 2033–2048.
Furnes, H., Shimron, A.E., Roberts, D., 1985. Geochemistry of Pan African volcanic arc sequences in southeastern Sinai and plate tectonic implications. Precambrian Research 29, 259–382.
Garfunkel, Z., 1999. History and paleogeography during the Pan-African orogen to stable platform transition: reappraisal of the evidence from the Elat area and the northern Arabian–Nubian Shield. Israel Journal of Earth Sciences 48, 135–157.
Genna, A., Nehlig, P., Le Goff, E., Guerrot, C., Shanti, M., 2002. Proterozoic tectonism of the Arabian Shield. Precambrian Research 117, 21–40.
Gertisser, R., Keller, J., 2003. Trace element and Sr, Nd, Pb and O isotope variations in medium-K and high-K volcanic rocks from Merapi volcano, central Java, Indonesia: evidence for the involvement of subducted sediments in Sunda arc magma genesis. Journal of Petrology 44, 457–489.
Ghoneim, M.F., Aly, S.M., El Baraga, M.H., 1985. Geochemistry of the Malhag metavolcanics, south Sinai Peninsula, Egypt. Annals of the Geological Survey of Egypt XV, pp. 171–182.
Goldstein, S.L., O'Nions, R.K., Hamilton, P.J., 1984. A Sm–Nd isotopic study of atmospheric dusts and particulates from major river systems. Earth and Planetary Science Letter 70, 221–236.
Green, R.O., 2006. Influence of slab thermal structure on basalt source region and melting conditions: REE and HFSE constraints from Garibaldi volcanic belt, northern Cascadia subduction system. Lithos 87, 23–49.
Greiling, R.O., Abdeen, M.M., Dardir, A.A., El Akhal, H., El Ramly, M.F., Kamal El Din, G.M., Osman, A.F., Rashwan, A.A., Rice, A.H.N., Sadek, M.E., 1994. A structural synthesis of the Proterozoic Arabian–Nubian Shield in Egypt. Geological Rundschau 83, 484–501.
Guo, Z.F., Hertogen, J., Liu, J.Q., Pasteels, P., Boven, A., Punzalan, L., He, H.Y., Luo, X.J., Zhang, W.H., 2005. Potassic magmatism in Western Sichuan and Yunnan Provinces, SE Tibet, China: petrological and geochemical constraints on petrogenesis. Journal of Petrology 46, 33–78.
Halpern, M., Tristan, N., 1981. Geochronology of the Arabian–Nubian Shield in southern Israel and eastern Sinai. Journal of Geology 89, 639–648.
Hargrove, U.S., Stern, R.J., Kimura, J.-I., Manton, W.I., Johnson, P.R., 2006. How juvenile is the Arabian–Nubian Shield? Evidence from Nd isotopes and pre-Neoproterozoic inherited zircon in the Bi'r Umq suture zone, Saudi Arabia. Earth and Planetary Science Letters 252, 308–326.
Hassanen, M.A., 1992. Geochemistry and petrogenesis of the Late Proterozoic Kid volcanics: evidence relevant to arc-intra-arc rifting volcanism in Southern Sinai, Egypt. Journal of African Earth Sciences 14, 131–145.
Humphris, S.E., 1984. The mobility of the rare earth elements in the crust. In: Henderson, P. (Ed.), Rare Earth Element Chemistry. Elsevier, Amsterdam, pp. 317–342.
Iacumin, M., Marzoli, A., El-Metawally, A.A., Piccirillo, E.M., 1998. Neoproterozoic dyke swarms from southern Sinai (Egypt): geochemistry and petrogenetic aspects. Journal of African Earth Sciences 26, 49–64.
Irvine, T.N., Baragar, W.R.A., 1971. A guide to the chemical classification of the common volcanic rocks. Canadian Journal of Earth Sciences 8, 523–548.
Jarrar, G., Wachendorf, H., Zachmann, D., 1993. A Pan-African alkaline pluton intruding the Saramuj conglomerate, South–West Jordan. Geological Rundschau 82, 121–135.
Jarrar, G., Stern, R.J., Saffarini, G., Al-Zubi, H., 2003. Late- and post-orogenic Neoproterozoic intrusions of Jordan: implications for crustal growth in the northernmost segment of the East African Orogen. Precambrian Research 123, 295–319.
Johnson, P.R., 2003. Post-amalgamation basins of the NE Arabian shield and implications for Neoproterozoic III tectonism in the northern East African orogen. Precambrian Research 123, 321–338.
Johnson, P.R., Woldehaimanot, B., 2003. Development of the Arabian–Nubian Shield: perspectives on accretion and deformation in the northern East African Orogen and the assembly of Gondwana. In: Yoshida, M., Dasgupta, S., Windley, B. (Eds.), Proterozoic East Gondwana: Supercontinent Assembly and Breakup: Journal of Geological Society, London, Special Publications, 206, pp. 289–325.
Katz, O., Avigad, D., Matthews, A., Heimann, A., 1998. Precambrian metamorphic evolution of the Arabian–Nubian Shield in the Roded area, southern Israel. Israel Journal of Earth Sciences 47, 93–110.
Katz, O., Beyth, M., Miller, N., Stern, R., Avigad, D., Basu, A., Anbar, A., 2004. A Late Neoproterozoic (630 Ma) Boninitic suite from southern Israel: implications for the consolidation of Gondwanaland. Earth and Planetary Science Letters 218, 475–490.
Kessel, R., Stein, M., Navon, O., 1998. Petrogenesis of late Neoproterozoic dikes in the northern Arabian–Nubian Shield implications for the origin of A-type granites. Precambrian Research 92, 195–213.
Kimura, J.I., Yoshida, T., 2006. Contributions of slab fluid, mantle wedge and crust to the origin of quaternary lavas in the NE Japan arc. Journal of Petrology 47, 2185–2232.
Kogiso, T., Omori, S., Maruyama, S., 2009. Magma genesis beneath Northeast Japan arc: a new perspective on subduction zone magmatism. Gondwana Research 16, 446–457.
Kolodner, K., Avigad, D., McWilliams, M., Wooden, J.L., Weissbrod, T., Feinstein, S., 2006. Provenance of north Gondwana Cambrian–Ordovician sandstone: U–Pb SHRIMP dating of detrital zircons from Israel and Jordan. Geological Magazine 143, 367–391.
Kröner, A., Eyal, M., Eyal, Y., 1990. Early Pan-African evolution of the basement around Elat, Israel, and the Sinai Peninsula revealed by single zircon evaporation dating, and implication of crustal accretion rates. Geology 18, 545–548.
Kröner, A., Kruger, J., Rashwan, A.A.A., 1994. Age and tectonic setting of granitoid gneisses in the Eastern Desert of Egypt and south-west Sinai. Geologische Rundschau 83, 502–513.
Küster, D., Liégeois, J.P., Matukov, D., Sergeev, S., Lucassen, F., 2008. Zircon geochronology and Sr, Nd, Pb isotope geochemistry of granitoids from Bayuda Desert and Sabaloka (Sudan): evidence for a Bayudian event (920–900 Ma) preceding the Pan-African orogenic cycle (860–590 Ma) at the eastern Boundary of the Saharan Metacraton. Precambrian Research 164, 16–39.
Le Bas, M.J., Le Maitre, R.W., Streckeisen, A., Zanettin, B., 1986. A chemical classification of volcanic rocks based on the total alkali–silica diagram. Journal of Petrology 27, 745–750.
Liégeois, J.P., Stern, R.J., 2010. Sr–Nd isotopes and the geochemistry of granite-gneiss complexes from the Meatiq and Hafafit domes, Eastern, Desert, Egypt: no evidence for pre-Neoproterozoic crust. Journal of African Earth Sciences 57, 31–40.
Ludwig, K.R., 2001a. User's manual for Isoplot/Ex version 2.05. Berkeley Geochronology Center, Special Publication No 1a, Berkeley, CA. 48 pp.
Ludwig, K.R., 2001b. SQUID 1.02: a user's manual. Berkeley Geochronology Center, Special Publication No. 2, Berkeley, CA. 19 pp.
Matthews, A., Reymer, A.P.S., Avigad, D., Cochin, J., Marco, S., 1989. Pressures and temperatures of Pan-African high-grade metamorphism in the Elat Association, NE Sinai. Israel Journal of Earth Sciences 38, 1–17.
Meert, J.G., 2003. A synopsis of events related to the assembly of eastern Gondwana. Tectonophysics 362, 1–40.
Mittlefehldt, D.W., Ravina, A., 1983. Petrology and trace element chemistry of the Shahira Pass pluton. Israel Geological Society Annual Meeting, 24–27 April 1983, Nazarat, Abstracts, pp. 60–61.
Moghazi, A.M., 2003. Geochemistry and petrogenesis of a high-K calc-alkaline Dokhan Volcanic suite, South Safaga area, Egypt: the role of late Neoproterozoic crustal extension. Precambrian Research 125, 161–178.
Moghazi, A.M., Andersen, T., Oweiss, G.A., El Bouseily, A.M., 1998. Geochemical and Sr–Nd–Pb isotopic data bearing on the origin of Pan-African granitoids in the Kid area, southeast Sinai, Egypt. Journal of the Geological Society of London 155, 697–710.
Moussa, H.E., 2003. Geologic setting, petrography and geochemistry of the volcanosedimentary succession at Gebel Ferani area, southeastern Sinai, Egypt. Egyptian Journal of Geology 47, 153–173.
Moussa, E.M.M., Stern, R.J., Manton, W.I., Ali, K.A., 2008. Shrimp zircon dating and Sm/Nd isotopic investigations of Neoproterozic granitoids, Eastern Desert, Egypt. Precambrian Research 160, 341–356.
Navon, O., Reymer, A.P.S., 1984. Stratigraphy, structures and metamorphism of Pan-African age in central Kid, southeastern Sinai. Israel Journal of Earth Science 33, 135–149.
Pearce, J.A., 1983. Role of the sub-continental lithosphere in magma genesis at active continental margins. In: Hawkesworth, C.J., Norry, M.J. (Eds.), Continental Basalts and Mantle Xenoliths. Shiva Publishing, Nantwich, pp. 158–185.
Pearce, J.A., 2008. Geochemical fingerprinting of oceanic basalts with applications to ophiolite classification and the search for Archean oceanic crust. Lithos 100, 14–48.
Pearce, J.A., Peate, D.W., 1995. Tectonic implications of the composition of volcanic arc magmas. Annual Reviews in Earth and Planetary Sciences 23, 251–285.
Peng, T., Wang, Y., Zhao, G., Fan, W., 2008. Bingxia Peng Arc-like volcanic rocks from the southern Lancangjiang zone, SW China: geochronological and geochemical constraints on their petrogenesis and tectonic implications. Lithos 102, 358–373.
Petrone, C.M., Francalanci, L., Carlson, R.W., Ferrari, L., Conticelli, S., 2003. Unusual coexistence of subduction-related and intraplatetype magmatism: Sr, Nd and Pb isotope and trace element data from the magmatism of the San Pedro–Ceboruco graben (Nayarit, Mexico). Chemical Geology 193, 1–24.
Plank, T., 2005. Constraints from thorium/lanthanum on sediment recycling at subduction zones and the evolution of continents. Journal of Petrology 46, 921–944.
Plank, T., Langmuir, C.H., 1998. The chemical composition of subducting sediment and its consequences for the crust and mantle. Chemical Geology 145, 325–394.
Polat, A., Hofmann, A.W., 2003. Alteration and geochemical patterns in the 3.7–3.8 Ga Isua greenstone belt, West Greenland. Precambrian Research 126, 197–218.
Polat, A., Hofmann, A.W., Münker, C., Regelous, M., Appel, P.W.U., 2003. Contrasting geochemical patterns in the 3.7–3.8 Ga pillow basalt cores and rims, Isua greenstone belt, Southwest Greenland: implications for postmagmatic alteration processes. Geochimica et Cosmochimica Acta 67 (3), 441–457.
Polat, A., Appel, P.W.U., Frei, R., Pan, Y., Dilek, Y., Ordóñez-Calderón, J.C., Fryer, B., Hollis, J.A., Raith, J.G., 2007. Field and geochemical characteristics of the

Mesoarchean (3075 Ma) Ivisaartoq greenstone belt, southern West Greenland: Evidence for seafloor hydrothermal alteration in supra-subduction oceanic crust. Gondwana Research 11, 69–91.
Reymer, A.P.S., 1983. Metamorphism and tectonics of a Pan-African terrain in southeastern Sinai. Precambrian Research 19, 225–238.
Reymer, A.P.S., Matthews, A., Navon, O., 1984. Pressure–temperature conditions in the Wadi Kid metamorphic complex: implications for the Pan-African event in SE Sinai. Contributions to Mineralogy and Petrology 85, 336–345.
Samuel, M.D., Moussa, H.E., Azer, M.K., 2001. Geochemistry and petrogenesis of Iqna Shar, a volcanic rocks, Central Sinai, Egypt. Egyptian Journal of Geology 45–2, 921–940.
Samuel, M.D., Be'eri-Shelvin, Y., Azer, M.K., Whitehouse, M.J., Moussa, H.E., 2011. Provenance of conglomerate clasts from volcano-sedimentary sequence at Wadi Rutig in Southern Sinai, Egypt as revealed by SIMS U–Pb dating of zircon. Gondwana Research 20, 450–464.
Schürmann, H.M.E., 1966. The Precambrian Along the Gulf of Suez and the Northern Part of the Red Sea. E.J. Brill, Leiden. 404 pp.
Seghedi, I., Downes, H., Pécskay, Z., Thirlwall, M., et al., 2001. Magma genesis in a subduction-related post-collisional volcanic arc segment: the Ukrainian Carpathians. Lithos 57, 237–262.
Seghedi, I., Downes, H., Szakács, A., Mason, P.R.D., Thirlwall, M.F., RoŞu, E., Pécskay, Z., Márton, E., Panaiotu, C., 2004. Neogene– Quaternary magmatism and geodynamics in the Carpathian–Pannonian region: a synthesis. Lithos 72, 117–146.
Shimoda, G., Tatsumi, Y., Nohda, S., Ishizaha, K., Jahn, B.M., 1998. Setouchi high-Mg andesites revisited: geochemical evidence for melting of subducting sediments. Earth and Planetary Science Letters 160, 479–492.
Shimron, A.E., 1975. Petrogenesis of the Tarr albitite–carbonatite complex, Sinai Peninsula. Mineralogical Magazine 40, 13–24.
Shimron, A.E., 1980. Proterozoic island arc volcanism and sedimentation in Sinai. Precambrian Research 12, 437–458.
Shimron, A.E., 1981. The Dahab mafic–ultramafic complex, southern Sinai Peninsula — a probable ophiolite of Late Proterozoic (Pan-African) age. Ofioliti 6, 161–164.
Shimron, A.E., 1983. The Tarr Complex revisited — folding, thrusts and mélanges in the southern Wadi Kid region, Sinai Peninsula. Israel Journal of Earth Sciences 32, 123–148.
Shimron, A., 1984. Evolution of the Kid Group, southeast Sinai Peninsula: thrusts, mélanges, and implications for accretionary tectonics during the late Proterozoic of the Arabian–Nubian Shield. Geology 12, 242–247.
Shimron, A.E., 1987. Pan-African metamorphism and deformation in the Wadi Kid region, SE Sinai Peninsula: evidence from porphyroblasts in the Um Zariq Formation. Israel Journal of Earth Sciences 36, 173–193.
Soliman, K.A., Tolba, M.E., El Manakhly, M.M., Madbouly, M.E., Hasan, M.M., Abd El Magid, E.A., Khyamy, A.A., Abd El Mola, A.F., Mohamed, H.A., 1992. Geology of the albitite rock, Wadi El Tarr, southern Sinai. Annals of the Geological Survey of Egypt XVIII, pp. 29–37.
Stein, M., Goldstein, S., 1996. From plume head to continental lithosphere in the Arabian–Nubian Shield. Nature 382, 773–778.
Stern, R.J., 1981. Petrogenesis and tectonic setting of Late-Precambrian ensimatic volcanic rocks, Central Eastern Desert of Egypt. Precambrian Research 16, 195–230.
Stern, R.J., 1994. Arc assembly and continental collision in the Neoproterozoic East African Orogen: implications for the consolidation of Gondwanaland. Annual Review of Earth and Planetary Sciences 22, 319–351.
Stern, R.J., 2002. Crustal evolution in the East African Orogen: a neodymium isotopic perspective. Journal of African Earth Sciences 34, 109–117.
Stern, R.J., Gottfried, D., 1986. Petrogenesis of a Late-Precambrian (575–600 Ma) bimodal suite in northern Africa. Contributions to Mineralogy and Petrology 92, 492–501.
Stern, R.J., Manton, W.I., 1987. Age of Feiran basement rocks, Sinai: implications for late Precambrian crustal evolution in the northern Arabian–Nubian Shield. Journal of the Geological Society of London 144, 569–575.
Stern, R.J., Gottfried, D., Hedge, C.E., 1984. Late Precambrian rifting and crustal evolution in the Northeastern desert of Egypt. Geology 12, 168–171.
Stern, R., Ali, K., Andresen, A., Wilde, S., Abu-El-Enien, M., Hassan, I., 2010a. Results of geochronological investigations in Sinai undertaken as part of the 2008 JEBEL Fieldtrip, pp. 46–51. In: Pease, V., Kadi, K., Kozdroj, W. (Eds.), JEBEL Project October 2009 Field Excursion to the Midyan Terrane, Kingdom of Saudi Arabia, with Reports on Research by Participants in the JEBEL Project: Saudi Geological Survey Technical Report SGS-TR-2010-2, p. 95.
Stern, R.J., Ali, K.A., Liegeois, J.P., Johnson, P.R., Kozdroj, W., Kattan, F.H., 2010b. Distribution and significance of pre-Neoproterozoic zircons in juvenile Neoproterozoic igneous rocks of the Arabian–Nubian Shield. American Journal of Science 310, 791–811.
Stoeser, D.E., Camp, V.E., 1985. Pan-African microplate accretion of the Arabian Shield. Geological Society American Bulletin 96, 817–826.
Stoeser, D.B., Frost, C.D., 2006. Nd, Pb, Sr, and O isotopic characterization of Saudi Arabian Shield terranes. Chemical Geology 226, 163–188.
Stolz, A.J., Vame, R., Wheller, G.E., Foden, J.D., Abbott, M.J., 1988. The geochemistry and petrogenesis of K-rich alkaline volcanics from the Batu Tara volcano, eastern Sunda Arc. Contributions to Mineralogy and Petrology 98, 374–389.
Stolz, A.J., Vame, R., Davies, G.R., Wheller, G.E., Foden, J.D., 1990. Magma source components in an arc–continent collision zone: the Flores–Lembata sector, Sunda Arc, Indonesia. Contributions to Mineralogy and Petrology 105, 585–601.
Sultan, M., Chamberlain, K.R., Bowring, S.A., Arvidson, R.E., Abu Zied, H., El Kaliouby, B., 1990. Geochronologic and isotopic evidence for involvement of pre-Pan-African crust in the Nubian Shield Egypt. Geology 18, 761–764.
Sun, S.S., McDonough, W.F., 1989. Chemical and isotopic systematics of oceanic basalts: implications for mantle composition and processes. In: Saunders, A.D., Norry, M.J. (Eds.), Magmatism in Ocean Basins: Journal of Geological Society, London, Special Publications, 42, pp. 313–345.
Turner, S., Sandiford, M., Foden, J., 1992. Some geodynamic and compositional constraints on "postorogenic" magmatism. Geology 20, 931–934.
Whitehouse, M.J., Windley, B.F., Ba-Bttat, M.A.O., Fanning, C.M., Rex, D.C., 1998. Crustal evolution and terrane correlation in the eastern Arabian Shield, Yemen: geochronological constraints. Journal of the Geological Society of London 155, 281–295.
Whitehouse, M.J., Stoeser, D.B., Stacey, J.S., 2001a. The Khida terrane geochronological and isotopic evidence for Paleoproterozoic and Archean crust in the eastern Arabian Shield of Saudi Arabia. Gondwana Research 4, 200–202.
Whitehouse, M.J., Windley, B.F., Stoeser, D.B., Al-Khirbash, S., Ba-Bttat, M.A.O., Haider, A., 2001b. Precambrian basement character of Yemen and correlations with Saudi Araba and Somalia. Precambrian Research 105, 357–369.
Wilde, S.A., Youssef, K., 2000. Significance of SHRIMP U–Pb dating of the Imperial Porphyry and associated Dokhan Volcanics, Gebel Dokhan, North Eastern Desert, Egypt. Journal of African Earth Sciences 31, 403–410.
Wilde, S.A., Youssef, K., 2002. A re-evaluation of the origin and setting of the Late Precambrian Hammamat Group based on SHRIMP U–Pb dating of detrital zircons from Gebel Umm Tawat, North Eastern Desert. Egypt. Journal of Geological Society, London 159, 595–604.
Willis, K.M., Stern, R.J., Clauer, N., 1988. Age and geochemistry of late Precambrian sediments of the Hammamat Series from the northeastern Desert of Egypt. Precambrian Research 42, 173–187.
Wilson, M., 1989. Igneous Petrogenesis. Unwin Hyman, London. 457 pp.
Winchester, J.A., Floyd, P.A., 1976. Geochemical magma type discrimination: application to altered and metamorphosed basic igneous rocks. Earth and Planetary Science Letters 28, 459–469.
Woodhead, J.D., Eggins, S.M., Johnson, R.W., 1998. Magma genesis in the New Britain island arc: further insights into melting and mass transfer processes. Journal of Petrology 39, 1641–1668.
Xie, L.W., Zhan, Y., Zhang, H., Sun, J., Wu, F., 2008. In situ dtermination of trace elements, U–Pb and Lu–Hf isotopes in zircon and beddeleyite. Chemical Science Bulletin 53, 1565–1573.